TEXTURE DEFECT DETECTION USING WAVELET TRANSFORMS

by

Ahmet Latif Amet

BS. in E.E., Boğaziçi University, 1992

Submitted to the Institute for Graduate Studies in
Science and Engineering in partial fulfillment of
the requirements for the degree of
Master of Science
in
Electrical and Electronic Engineering

Boğaziçi University

1997

ACKNOWLEDGMENTS

I am very grateful to my thesis supervisor Assoc. Prof. Dr. Ayşın Ertüzün for being dedicated to give me any kind of support whenever I needed. Her interest and kindness was the actual drive for me during the course of this study.

I would like to express my thanks to Prof. Dr. Aytül Erçil for her help and useful suggestions.

I would like to express my thanks to Prof. Dr. Bülent Sankur for participating to examining committee.

I would like to express my gratitude to Prof. Dr. Yorgo Istefanopulos as being my advisor during M.S. study and the person introducing me into signal processing.

Last but not least, my thanks are due to my family for their patience and understanding in all phases of this thesis.

ABSTRACT

In recent years, achievements obtained in machine vision were on the way to facilitate computers replace several tasks heretofore performed by humans. Among those tasks, visual inspection of textile fabrics is one of importance. Inspection is performed by detecting and recording the position of defected parts in a roll of textile web. Textile fabric images carry textural properties. Therefore, texture analysis methods can be incorporated to device algorithms for the solution of the defect detection problem. Wavelet transforms have proven to constitute powerful means suitable for several image processing applications. In this thesis, wavelet transform based feature extraction methods are investigated in detail. Pyramid structured wavelet transform (PSWT), wavelet packet (WP) expansion and multichannel features are compared with features derived from spatial domain co-occurrence matrices in terms of defect detection capacity. Finally, a novel feature extraction scheme called subband domain co-occurrence matrices is proposed and compared computationally and performance-wise with the rest.

KISA ÖZET

Son yıllarda yapay görmede elde edilen gelişmeler bugüne kadar insanlarca gerçekleştirilen birçok görevin yerini bigisayarların alması yönünde olmuştur. Bu görevlerden tekstil ürünlerinin görsel kontrolü önemli birini teşkil etmektedir. Kontrol kumaş topu üzerindeki hatalı bölgelerin saptanması ve kaydedilmesi şeklinde olmaktadır. Tekstil imgeleri doku özellikleri taşımaktadır. O halde, doku analiz metodları hata saptama probleminin çözümü için algoritmalar geliştirilmesinde kullanılabilirler. Dalgacık dönüşümünün çeşitli imge işleme uygulamaları için uygun, etkin bir araç olduğu ispatlanmıştır. Bu tezde dalgacık dönüşümüne dayalı öznitelik bulma metodları derinlemesine incelenmektedir. Piramid yapılı dalgacık dönüşümü, dalgacık paket açılımı ve çoklu kanal öznitelikleri uzamsal alan co-occurrence matrislerinden elde edilen özniteliklerle hata saptama kapasitesi açısından karşılaştırılmaktadır. Son olarak, altband alan co-occurrence matrisleri adı verilen yeni bir öznitelik bulma yöntemi önerilmekte ve hesaplama karmaşıklığı ve başarım açısından kalanlarla kıyaslanmaktadır.

TABLE OF CONTENTS

LIST OF FIGURES

LIST OF TABLES

ABBREVIATIONS

ASM	Angular Second Moment
CCD	Charge Coupled Device
CON	Contrast
DCT	Discrete Cosine Transform
DFT	Discrete Fourier Transform
DST	Discrete Sine Transform
ENT	Entropy
FFT	Fast Fourier Transform
HH	High-High Frequency Band
HL	High-Low Frequency Band
IDM	Inverse Difference Moment
LH	Low-High Frequency Band
LL	Low-Low Frequency Band
MRF	Markov Random Fields
PSWT	Pyramid-Structured Wavelet Transform
SAR	Simultaneous Autoregressive Model
SBCM	Subband Domain Co-occurrence Matrices
SBMRF	Subband Domain Markov Random Fields
SDCM	Spatial Domain Co-occurrence Matrices
SOC	System Operating Curve
WP	Wavelet Packet
WPS	Wavelet Packet Signatures
WT	Wavelet Transform

1. INTRODUCTION

1.1. Problem Statement

Visual inspection, which constitutes an important part of the quality control of industrial products, is a cumbersome task. Especially in plants, where the production line speeds are high as paper, metal, and textile industries or involving processes which do not enable human intervention during assembly this becomes a real problem. Until recent years, this job was heavily relied upon human inspectors. Development of fast and specialized hardware equipment however, facilitated the applicability of image processing and machine vision tools for the solution of real world problems in a broad area of industry. Among those where automated visual inspection has found great base was the textile industry. Reasons for that are quite simple. Inspection of roll of web textile fabrics is time-consuming and/or boring for humans to perform. Also, it has been reported that human visual inspection is, at best, 80 per cent effective, and, furthermore this effectiveness can only be achieved if a rigidly structured set of inspection checks is implemented [1].

Visual inspection of textile fabrics is mainly concerned with the detection of any defects or anomalies in the visual appearance of the outcoming rolling web product and registration of the location and type of those imperfections and degradations in order to be used when preparing the final product for the market. Therefore, an automated visual inspection system performing those tasks will be made up of two major parts: (1) the sensing part and (2) the processing part.

Sensing, although alternative strategies as laser scanning [2], or ultrasound systems [3] have been applied, is most frequently performed with Charge Coupled Device (CCD) cameras. But most important component of the sensing is illumination. For appropriate image acquisition, lighting source and topology selection, especially in the factory environment, often needs great care.

The processing part, on the other hand, depending on the complexity of the system varies from general purpose computer to customized hardware and from a single block system performing defect detection only to more sophisticated one, as that proposed by Brzakovic and Vujovic (Figure 1.1), performing defect type classification as well [4].

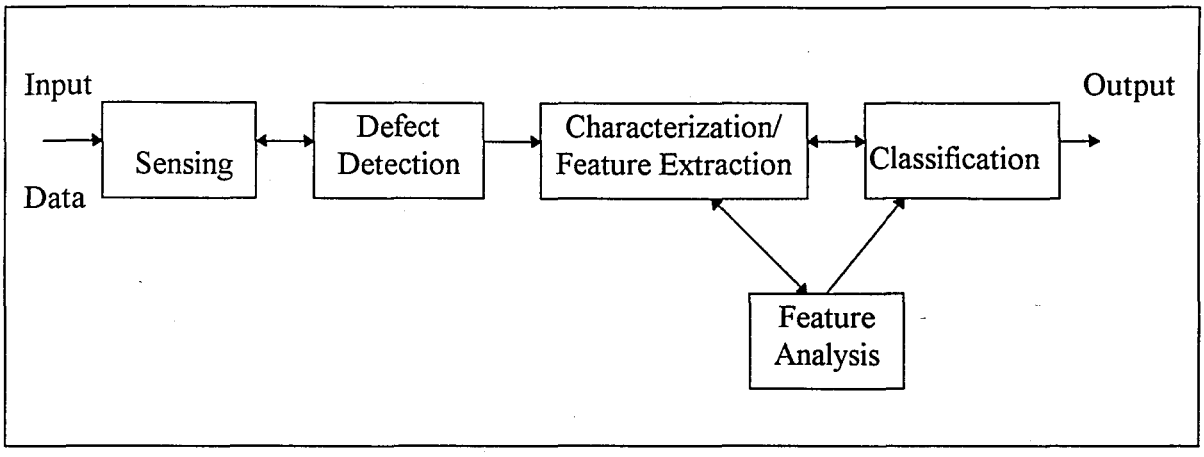

FIGURE 1.1. A general inspection system

This thesis is concerned with the defect detection problem of textured images. During the last three decades, texture analysis problems have always been an active research topic for the image processing society. Numerous algorithms have been devised in the efforts of representation of textures. In the late seventies and early eighties, most of the texture analysis methods were based on the first and second order statistics of the image gray values. Features used were derived from co-occurrence matrices, run-length matrices or obtained directly from the gray values as autocorrelation function. In mid-eighties, model based methods have appeared as an alternative. Textures were considered as realization of stochastic processes and parameters of the distribution estimated through pattern analysis algorithms have served as features for the quantitative description of textures. Towards the end of eighties, wavelet transforms have emerged as an efficient tool for multiscale/multiresolution image representation. Advantages of multiresolution analysis have been widely investigated. In this thesis, different texture analysis methods based on multifrequency/multiresolution features which were used for classification, identification

and segmentation of textured images are applied to the solution of the texture defect detection problem. Namely, features obtained from pyramid structured wavelet decomposition, wavelet packet expansion and multichannel filtering of textured images are compared with features derived from spatial domain co-occurrence matrices in terms of defect detection capacity. Extensive experimental tests are carried on database provided by Altınyıldız A.Ş. consisting of digital images of all possible defect types acquired in the real factory environment where such an inspection system is expected to operate. Finally a novel feature extraction scheme combining wavelet transform and co-occurrence matrices and called subband domain co-occurrence matrices is proposed and compared computationally and performance-wise with the rest.

1.2. Outline of the Thesis

The organization of this thesis is as follows:

In chapter two the texture analysis methods are reviewed and the theoretical background of the problem is established.

Chapter three starts with a brief survey on texture defect detection and continues with a general description of the system that is used for evaluation of the feature extraction algorithms which are presented each separately in the sequel. Implementation details and experimental results for five different algorithms based on pyramid-structured wavelet transform, wavelet packet expansion, multichannel filtering, spatial domain co-occurrence matrices and subband domain co-occurrence matrices are provided along with each method. It concludes with the comparison of the presented detection schemes.

Chapter four concludes the thesis and comments about the possible directions of future work on the subject.

2. TEXTURE ANALYSIS

2.1. Introduction

Before going into detail about texture analysis and discussing the methods developed in so far, we think this is the right place to clarify what is meant by texture. It is difficult to make a unique definition of texture. Since the early seventies, in the attempts to describe texture, several definitions of texture has appeared in the literature. According to Hawkins "The notion of texture appears to depend upon three ingredients: (i) some local 'order' is repeated over a region which is large in comparison to the orders size, (ii) the order consists in the nonrandom arrangement of elementary parts, and (iii) the parts are roughly uniform entities having approximately the same dimensions everywhere within the textured region"[5]. Horn [6] considers texture to be "detailed structure in an image that is too fine to be resolved, yet coarse enough to produce a noticeable fluctuation in the gray levels of neighboring cells." Another definition due to Sklansky is "A region in an image has a constant texture if a set of local statistics or other local properties of the picture function are constant, slowly varying, or approximately periodic" [7]. The difficulty in providing a commonly accepted definition for texture is apparent from the diversity of the mathematical models that has emerged in the past two decades. If we review the vision literature we can find as many definitions for texture as many approaches to model it or as many different applications it has found in the vision research world.

From our point of view (i.e., visual inspection), we will define texture, very informally, as "the tactile quality of the surface" since any disorder or anomaly in it is meant degradation of quality and nonconformity of the product.

As texture is important characteristic of the images it is used in a number of applications and has been a subject of intense study by many researchers. One such an application is the recognition of image regions using texture properties. Psychophysical

studies prompt the importance of texture in identifying such homogeneous regions by the human brain. Determining the class in which each uniform region in an image belongs to is called *texture classification*. Finding the boundaries of the homogeneous regions however, is the second type of problem that texture analysis research attempts to solve. This is called *texture segmentation*. The goal of texture segmentation is to find the boundary map of the textured regions in an image. Some other applications that use texture analysis as a means are: image compression, extraction of 3D-shape from texture, and detection of the defective regions in textured images which is the subject of this study. In this respect, in the subsequent sections we review the texture analysis tools and develop the quantitative measures of texture.

2.2. Texture Analysis Methods

In the preceding section, we tried to provide a qualitative description for texture. Such descriptions, although seem to be reasonable and are essential as a starting point, they do not immediately lead to quantitative measures. But, what they point out is that, in describing textures, most often we refer to some perceived qualities as uniformity, roughness, coarseness, density, regularity, linearity, directionality, frequency and phase. Analysis of textures is an attempt of mathematical formulation of those perceived qualities. Methods developed for this purpose can be collected under four main categories:(i) statistical methods, (ii) geometrical methods (iii) model based methods and (iv) signal processing methods [8].

2.2.1. Statistical Methods

In statistical methods, features are derived from the first or second order statistics of the texture gray level values. Measures used are co-occurrence matrices, autocorrelation

function, run-length matrices, and neighboring gray level dependence matrices. They have been primarily used for texture classification purposes. A review can be found in [8-10].

2.2.2. Geometrical Methods

Geometrical methods, assume texture to be composed of primitives, namely, "texture elements" or as Julesz has called "textons" and analyze the geometrical properties of these structured components. Textures are described either by features derived from the statistical properties of those elements or the placement rule extracted from the texture where the primitives are inherent using geometrical or syntactic methods. Studies of Zucker *et al.* [11] and Tomita *et al.* [12] are examples of structural texture analysis .

2.2.3. Model-Based Methods

Model based methods, assume textured images as realizations or samples from parametric probability distributions on the image space, and try to fit simultaneous autoregressive models (SAR), Markov random field (MRF) models [13-17], and fractal models [18] to the textured image. Model parameters are used as features in the classification and segmentation problems. Advantage of this method over other statistical methods is that the model parameters can be used not only to describe the texture but also to synthesize it. They have been used for classification, segmentation and compression of textured images.

2.2.4. Signal Processing Methods

Signal processing methods, try to derive features from the filtered images which will resemble certain textural properties. Psychophysical experiments has shown that methods based on spatial-frequency domain features are plausible with the human visual system.

In recent years, by the development of the wavelet theory this method has received special interest. Number of algorithms based on wavelet transform [19],[20] and gabor filters [21], [22-27] have been proposed for classification and segmentation of textured images. In the following sections we present the theory of the methods that we have applied to our problem.

2.3. Spatial Gray Level Co-occurrence Matrices

Among all statistical methods, the most popular one which is based on the estimation of the second order statistics of the spatial arrangement of the gray values, is the gray level co-occurrence matrices (SGLCM). Julesz [28] was first to use co-occurrence statistics in the human texture discrimination experiments. A co-occurrence matrix is a square matrix with elements corresponding to the relative frequency of occurrence of pairs of gray level of pixels separated by a certain distance in a given direction. Formally, the GxG gray level co-occurrence matrix $P_{\mathbf{d}}$ for a displacement vector $\mathbf{d} = (dx,dy)$ is defined as

$$P_{\mathbf{d}}(i,j) = |\{ ((r, s), (t, v)) : I(r, s) = i, I(t, v) = j \}| \tag{2.1}$$

where $I(\cdot,\cdot)$ denotes an image of size NxN with G gray values, (r, s), $(t, v) \in NxN$, $(t,v) = (r + dx, s + dy)$ and $|.|$ is the cardinality of a set.

As an example, lets consider the following 4x4 image with four gray values,

0	0	1	1
0	0	1	1
0	2	2	2
2	2	3	3

FIGURE 2.1. Example image

The 4x4 gray level co-occurrence matrix for that image with a displacement vector of **d**=(1,0) is given by

$$P_d = \begin{bmatrix} 2 & 2 & 1 & 0 \\ 0 & 2 & 0 & 0 \\ 0 & 0 & 3 & 1 \\ 0 & 0 & 0 & 1 \end{bmatrix}$$

If we calculate the co-occurrence matrix for **-d**, which is nothing but the transpose of P_d, and add the two matrices, then we get a symmetric matrix and it contains spatial gray level co-occurrences of pixels in the horizontal direction with separation distance one as it is given below.

$$P_H = P_d + P_{-d} = P_d + P_d{}^T = \begin{bmatrix} 4 & 2 & 1 & 0 \\ 2 & 4 & 0 & 0 \\ 1 & 0 & 6 & 1 \\ 0 & 0 & 1 & 2 \end{bmatrix}$$

Similarly by choosing appropriate displacement vector, one can calculate co-occurrence matrices for different directions and pixel separation distances. Here in below we give the co-occurrence matrices for the above example image calculated for distance one and angles of 45, 90 and 135 degrees.

$$P_{45} = \begin{bmatrix} 4 & 1 & 0 & 0 \\ 1 & 2 & 2 & 0 \\ 0 & 2 & 4 & 1 \\ 0 & 0 & 1 & 0 \end{bmatrix}, \quad P_{90} = \begin{bmatrix} 6 & 0 & 2 & 0 \\ 0 & 4 & 2 & 0 \\ 2 & 2 & 2 & 2 \\ 0 & 0 & 2 & 0 \end{bmatrix}, \quad P_{135} = \begin{bmatrix} 2 & 1 & 3 & 0 \\ 1 & 2 & 1 & 0 \\ 3 & 1 & 0 & 2 \\ 0 & 0 & 2 & 0 \end{bmatrix}$$

These form an adequate set to extract features for most of the textures. Haralick, Shanmugan and Dinstein [29] proposed 14 measures of textural features which are derived

from the co-occurrence matrices, and each represent certain image properties as coarseness, contrast, homogeneity and texture complexity. Those that we used for extracting features in the defect detection of textured images are:

1) Entropy : $$\text{ENT} = -\sum_i \sum_j p(i,j) \log p(i,j) \tag{2.2}$$

Entropy gives a measure of complexity of the image. Complex textures tend to have higher entropy.

2) Contrast : $$\text{CON} = \sum_i \sum_j (i-j)^2 p(i,j) \tag{2.3}$$

Contrast feature is a measure of the image contrast or the amount of local variations present in an image.

3) Angular Second Moment : $$\text{ASM} = \sum_i \sum_j \{p(i,j)\}^2 \tag{2.4}$$

Angular second moment is a measure of the homogeneity of an image. Hence it is a suitable measure for detection of disorders in textures. For homogeneous textures value of angular second moment turns out to be small compared to non-homogeneous ones.

4) Inverse Difference Moment : $$\text{IDM} = \sum_i \sum_j \frac{1}{1+(i-j)^2} p(i,j) \tag{2.5}$$

In above Eqs. (2.2) to (2.5), $p(i,j)$ refers to the normalized entry of the co-occurrence matrices. That is $p(i,j) = P(i,j)/R$ where R is the total number of pixel pairs (i,j). For a displacement vector $\mathbf{d} = (dx, dy)$ and image of size NxM R is given by $(N-dx)(M-dy)$.

Co-occurrence matrices are from the oldest textural feature extraction methods. They were used in various texture analysis and classification problems [30]. The most

prominent disadvantage with this method is that there is no well established feature selection algorithm. Certain features with certain displacement performing well in one type of textures may fail in others. Most often in the application, features to be used are determined experimentally. But, it has been reported by Weszka *et al.* [31] that co-occurrence features performed better than features obtained from a 2-D Fourier power spectrum. Ohanian and Dubes [32] also conducted a comparative study on Markov Random Field parameters, Gabor multi-channel features, fractal based features and co-occurrence features. They found co-occurrence features to outperform the former three. In this thesis we performed an analogous study for texture defect detection.

2.5. Wavelet Transforms

Wavelets, although were known for many years, received the attention of the image processing society only after the papers of Daubechies [33], who provided the discretization of the wavelet transform, and Mallat [34] who established the connection between multiresolution theory and wavelet transforms. In this section, we provide the theory about discrete wavelet transform and decomposition of a signal using wavelet filters.

The wavelet transform is defined as a decomposition of a signal with a family of real orthonormal bases $\psi_{m,n}(x)$ obtained through translation and dilation of a kernel function $\psi(x)$ known as the mother wavelet.

$$\psi_{m,n}(x) = 2^{-m/2}\psi(2^{-m}x - n) \tag{2.6}$$

where m and n are integers. Since $\psi_{m,n}(x)$ form an orthonormal set, the analysis and synthesis formula for a signal $f(x)$ are, respectively, given by

$$c_{m,n} = \int_{-\infty}^{+\infty} f(x)\psi_{m,n}(x)dx \tag{2.7}$$

$$f(x) = \sum_{m,n} c_{m,n}\psi_{m,n}(x) \tag{2.8}$$

Here in, the formula we use are for wavelet transform coefficients discretized on a dyadic scale. For continuous case and more about theory the reader may refer to [33] and [34]. The mother wavelet can be constructed first determining a scaling function satisfying the two-scale difference equation

$$\phi(x) = \sqrt{2}\sum_{k} h(k)\phi(2x-k) \tag{2.9}$$

and then relating $\psi(x)$ to the scaling function via

$$\psi(x) = \sqrt{2}\sum_{k} g(k)\phi(2x-k) \tag{2.10}$$

where

$$g(k)=(-1)^k h(1-k). \tag{2.11}$$

In order to have wavelet bases obtained through the above procedure be unique, orthonormal and have desired regularity, the coefficients $h(k)$ have to meet certain conditions. Here we do not go into details of designing those filters. Several set of coefficients satisfying those requirements can be found in the literature (see Table 2.1).

Nice thing about this decomposition scheme is that one does not need to calculate explicitly the scaling and mother wavelet functions, but can obtain the transform coefficients recursively using $h(k)$ and $g(k)$. Lets consider a J- level decomposition. This can be written as

$$\begin{aligned} f(x) &= \sum_{k} c_{0,k}\phi_{0,k}(x) \\ &= \sum_{k}(c_{J+1,k}\phi_{J+1,k}(k) + \sum_{j=0}^{J} d_{j+1,k}\psi_{j+1,k}(x)) \end{aligned} \tag{2.12}$$

where coefficients $c_{0,k}$ are given and coefficients $c_{j+1,n}$ and $d_{j+1,n}$ at scale $j+1$ are related to the coefficients $c_{j,n}$ at scale j via

$$c_{j+1,n} = \sum_k c_{j,k} h(k-2n)$$
$$d_{j+1,n} = \sum_k d_{j,k} g(k-2n) \qquad (2.13)$$

for $0 \le j \le J$. In signal processing terms operations in Eq. (2.13) is nothing but convolving coefficients $c_{j,n}$ and $d_{j,n}$ at resolution j with $\tilde{h}(n)$ and $\tilde{g}(n)$ and downsampling by two (dropping every other sample) to obtain $c_{j+1,n}$ and $d_{j+1,n}$. Here $\tilde{h}(n)$ and $\tilde{g}(n)$ are defined as

$$\tilde{h}(n) = h(-n), \quad \tilde{g}(n) = g(-n)$$

and can be regarded as impulse responses of quadrature mirror lowpass and highpass filters H and G, respectively. The output of J-level decomposition will contain the low-resolution coefficient $c_{J,n}$ and detail coefficients $d_{j,n}$ for each level ($1 \le j \le J$) (Figure 2.2). In the synthesis, the procedure works opposite, i.e., the low-resolution coefficient $c_{J,n}$ and detail coefficients $d_{j,n}$ are first upsampled by two (inserting a zero between neighboring samples) and then filtered with $h(n)$ and $g(n)$ respectively.

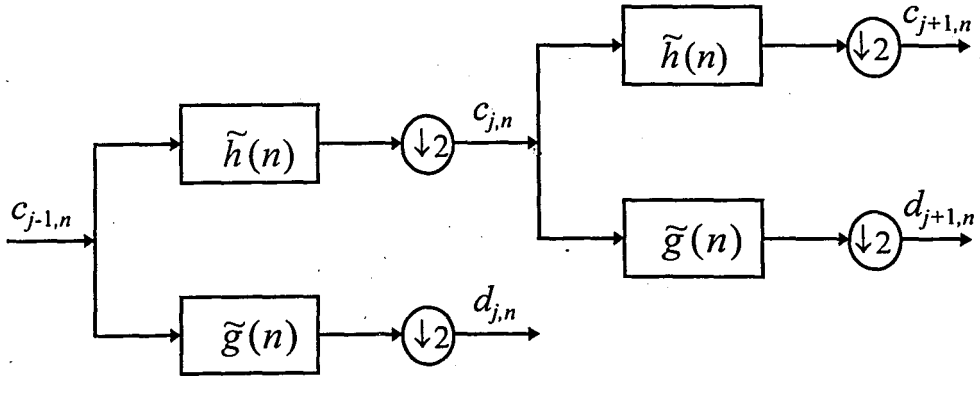

FIGURE 2.2. Two-level wavelet decomposition shceme

TABLE 2.1. Wavelet Filter Coefficients

Coefficient	Battle-Lemarie	16-tap Daubechies
$h(0)$	0.766130	0.054416
$h(1)$	0.433923	0.312872
$h(2)$	-0.050202	0.675631
$h(3)$	-0.110037	0.585355
$h(4)$	0.032081	-0.015829
$h(5)$	0.042068	-0.284016
$h(6)$	-0.017176	0.000472
$h(7)$	-0.017982	0.128747
$h(8)$	0.008685	-0.017369
$h(9)$	0.008201	-0.044088
$h(10)$	-0.004354	0.013981
$h(11)$	-0.003882	0.008746
$h(12)$	0.002187	-0.004870
$h(13)$	0.001882	-0.000392
$h(14)$	-0.001104	0.000675
$h(15)$	-0.000927	-0.000117

Decomposition in the conventional wavelet transform scheme which is also called pyramid structured wavelet transform is carried recursively on the output of filter $\tilde{h}(n)$. This, in signal processing terms, is equivalent to splitting each time the low-frequency band (Figure 2.3.a). For signals with most of their energy concentrated in the low frequency regions this is suitable. For analyzing signals with dominant energy at the middle frequencies, however, the concept of wavelet bases was generalized to contain a set of modulated waveform orthonormal bases, called wavelet packets. The library of wavelet packets $\{W_n\}_{n=0}^{\infty}$ can be generated from a given function W_0 as follows:

$$W_{2n}(x) = \sqrt{2}\sum_k h(k)W_n(2x-k) \tag{2.14}$$

$$W_{2n+1}(x) = \sqrt{2}\sum_k g(k)W_n(2x-k) \tag{2.15}$$

where $W_0(x)=\phi(x)$ and $W_1(x)=\psi(x)$. Therefore the library of wavelet packets bases can be defined as collection of orthonormal bases composed of functions of the form $W_n(2^p x-k)$ where $p \in Z$ is scale index, $k \in Z$ localization index, and $n \in N$ is oscillation index.

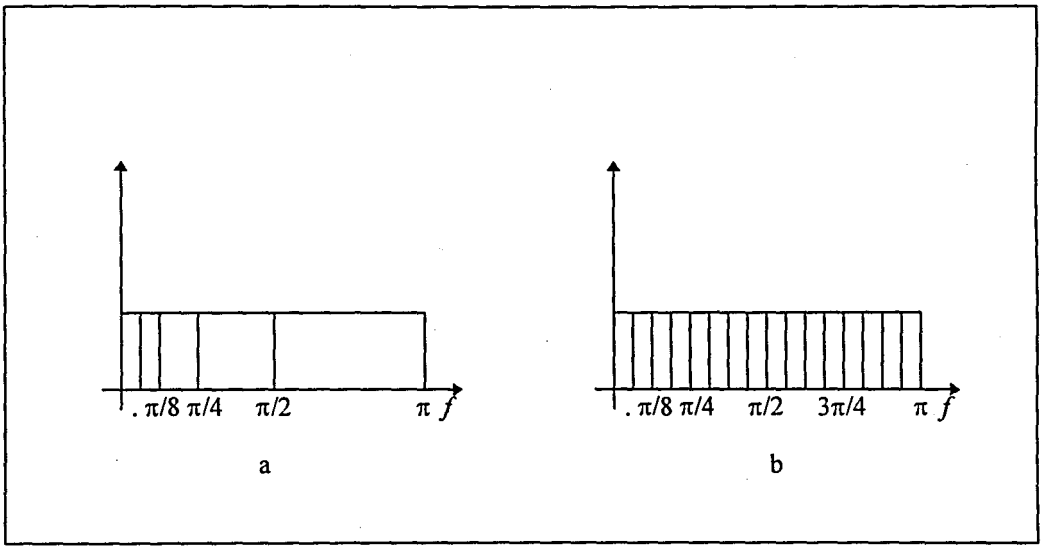

FIGURE 2.3. Split of frequency band for 4-level decomposition with (a) Pyramid structured wavelet transform and (b) wavelet packet bases.

Extension of wavelet transform (or wavelet packets) to 2-D is achieved by expressing the 2-D basis functions as tensor product of two 1-D wavelet (or wavelet packet) basis functions along the horizontal and vertical directions. The corresponding filter coefficients can be computed via

$$h_{LL}(k,l)=h(k)h(l), \qquad h_{LH}(k,l)=h(k)g(l),$$

$$h_{HL}(k,l)=g(k)h(l), \qquad h_{HH}(k,l)=g(k)g(l).$$

Wavelet packet expansion, algorithmically corresponds to subband decomposition and is numerically as fast as the FFT [35]. This makes them appealing for many image processing applications. Laine and Fan [19] used energy and entropy calculated from wavelet packet expansion of images for classification of textures. They compared different subsets of the wavelet packet bases in terms of performance and reported classification rates of 99-100 per cent. Chang and Kuo [20] used a tree-structured wavelet decomposition (which is equivalent to wavelet packet expansion) to classify textures. They reached up 98 to 99 per cent classification accuracy on a database consisting of 30 textures from Brodatz's texture album.

The important point in wavelet packet expansion of an image is the selection of the best basis set that will capture as much information about texture spectral properties as to achieve the desired performance. Measures proposed to extract the optimal quadtree are channel energy [20], entropy [35], class separability [36], and subband coding gain [37].

Finally, we will mention some of the virtues of wavelet transform (WT) over other transforms as discrete cosine transform (DCT), discrete sine transform (DST) and discrete fourier transform (DFT). This will explain why WT, though new compared to the latter, become so popular and used in such a wide range of image processing applications ranging from segmentation to classification problems and from compression to detection algorithms. The wavelet transform of an image generates a data structure known as scale-space representation. In this representation, spatial/spatial-frequency resolution is not fixed as in DCT, DST and DFT, but change in an optimal way. Namely, the spatial resolution increases with frequency, and spatial-frequency resolution becomes narrower as frequency decreases. So high frequency signals are precisely located in spatial domain, while the low-frequency signals are precisely located in the frequency domain. Sharp edges, which are well localized spatially and have a significant high frequency content, can be represented more compactly by WT than the other transforms. Furthermore, WT is computationally attractive, and does not introduce redundancy. An image can be represented in multiple resolutions by the same amount of data with the original form (Figure 2.4).

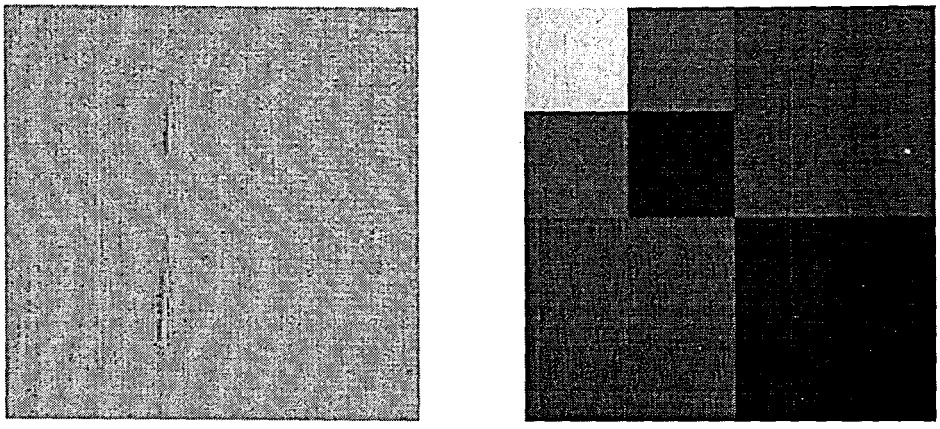

FIGURE 2.4. A textile fabric image (left) and its wavelet transform (right)

2.6. 2-D Gabor Filters

A Gabor function is a complex sinusoid grating of a certain frequency and orientation modulated by a Gaussian envelope. It was introduced by Gabor [38] in 1-D and later extended to 2-D by Daugman [39]. Formally, a 2-D complex Gabor function is expressed as:

$$h(x,y) = g(x',y')\exp[j2\pi(Ux+Vy)] \tag{2.16}$$

where $(x',y') = (x\cos\phi + y\sin\phi, -x\sin\phi + y\cos\phi)$ are rotated spatial domain rectilinear coordinates, and $g(x,y)$ is a 2-D Gaussian function as:

$$g(x,y) = \left(\frac{1}{2\pi\lambda\sigma^2}\right)\cdot\exp\left[-\frac{(x/\lambda)^2+y^2}{2\sigma^2}\right]. \tag{2.17}$$

with aspect ratio λ, and scale parameter σ and ϕ angle from the x-axis. The spatial frequency response of the Gabor function (2.16) is

$$H(u,v) = \exp\left\{-2\pi^2\sigma^2\left[(u'-U')^2\lambda^2 + (v'-V')^2\right]\right\} \tag{2.18}$$

where $(u',v') = (u\cos\phi + v\sin\phi, -u\sin\phi + v\cos\phi)$ and (U',V') is a similar rotation of the center frequency (U, V). Thus $H(u,v)$ is a bandpass Gaussian with minor axis oriented at an angle ϕ from the u-axis aspect ratio $1/\lambda$ radial frequency $F = \sqrt{U^2 + V^2}$ (measured in cycles/image-width) and orientation $\theta = \tan^{-1}(V/U)$ (degrees or radians from the u-axis). Generally it is considered to be more convenient to let modulating Gaussians have same orientation with the complex sinusoidal grating [23] (i.e $\phi=\theta$). Then (2.16) and (2.18) reduce to

$$h(x,y) = g(x',y')\exp[j2\pi Fx')] \tag{2.19}$$

and

$$H(u,v) = \exp\left\{-2\pi^2\sigma^2\left[(u'-F)^2\lambda^2 + (v')^2\right]\right\}. \tag{2.20}$$

The filter given by (2.19) has a bandpass nature. Its half-peak radial and orientation bandwidths are defined as: $B = \log_2[(\pi F\lambda\sigma+\alpha)/(\pi F\lambda\sigma-\alpha)]$ and $\Omega = 2\tan^{-1}[\alpha/(\pi F\sigma)]$ respectively, where $\alpha = \sqrt{\ln 2/2}$ and measured in octaves and radians or degrees. By proper selection of the free parameters B, F, Ω and θ Gabor filters can be tuned to any arbitrary frequency and orientation. In Figure 2.5 we provide the impulse and frequency responses of a Gabor filter tuned to $(B,\Omega, F, \theta)=(1, \pi/4, 8, 0)$.

Therefore, since the Gabor function is of bandpass nature, passing an image through a Gabor filter amounts to suppressing image patterns with frequency and orientation content other than those at which filter has been tuned. For a demonstration of the spatial/spatial-frequency selectivity of Gabor filters see Figure 3.12 in section 3.5.

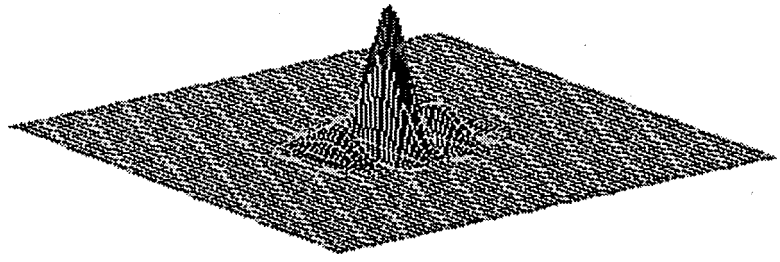

(a)

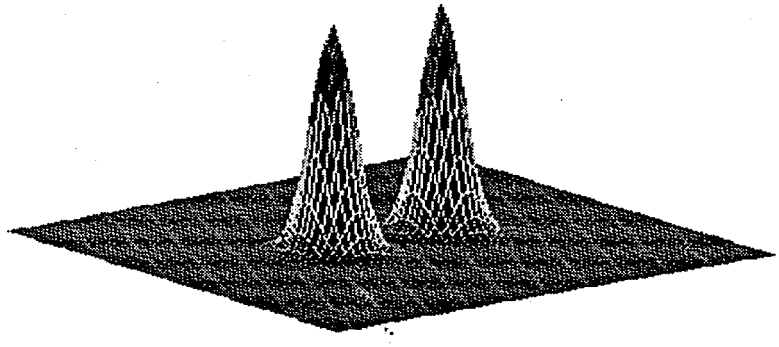

(b)

FIGURE 2.5. (a) Impulse and (b) frequency responses of an even symmetric Gabor filter with $(B,\Omega, F, \theta)=(1, \pi / 4, 8, 0)$

Gabor function since its extension to 2-D, was used in a number of image processing applications. This is due to the unique properties it possesses. Some of those properties which make it especially suitable for texture analysis are:

1) Gabor functions are the only functions to achieve the lower bound of the space-bandwidth product as specified by the uncertainty principle [39]. This means they can simultaneously be optimally localized in spatial and spatial-frequency domains. Thus, they make possible design of filters showing high frequency selectivity while possessing good spatial localization.

2) Gabor functions resemble the receptive field profiles of the simple cells in the human visual system [40], [41].

3) They are bandpass filters. Thus, they can be configured to extract specific band of frequency contents from an image.

3. TEXTURE DEFECT DETECTION

3.1. General Overview

Texture defect detection, in its own, is a broad field. It has two variables. The underlying texture's characteristic and the type of the defects. Most often methods that perform well in one type of textures or defects fail in others. Therefore before developing an algorithm these two variants should be well defined.

Texture defects can be classified into three categories: geometrical defects, intensity defects and a mixture of both. A geometrical defect is a distortion which results from a spatial arrangement of pixel values and does not considerably change the local gray level histogram. So for such defects methods based on the local first order statistical features does not work. Intensity defects on the other hand, are those which induce remarkable change in the local intensity. Further, texture imperfections can be classified according to their extend as localized and extended. For a complete study reader may refer to [42].

Majority of the existing texture defect detection schemes are in the domain of textile inspection. Detection of defects in textile fabrics is a difficult problem. This has two reasons. First, textile fabric images are characterized by complex textures. Second, the defect types occupy a wide spectrum. They vary from intensity defects to geometrical and from localized ones to extended. So for such textures simple thresholding techniques do not yield satisfactory results. Algorithms used for defect detection of this type of textures involve more sophisticated methods. Dewaele *et al.* [43] used signal processing methods to detect point and line defects in texture images. Their technique used convolution filters whose spatial form adapted to the textures for inspection. Specifically the filter size was based on an estimate of the repetitiveness of the pattern. Filter coefficients were computed using the eigenvectors of a covariance matrix for several image points. Cohen *et al.* [44] inspected textile fabrics for defects through the use of stochastic texture model, namely the

Gaussian Markov Random fields. Defects were detected using likelihood ratio tests in nonoverlapping windows within the image. To improve the execution time they have used sufficient statistics of the model parameters. Neubauer [45] developed a segmentation algorithm to be used for detection of defects in textile fabrics. His method involved first filtering the image and then evaluating the filtered images using a histogram calculated in windows within the image. Finally, textures were classified using a perceptron net which was trained by backpropagation on the sample images containing defects. Chen and Jain [46] on the other hand, used a structural approach to detect defects in textured images. They extract a skeletal structure from images and by detecting the anomalies in certain statistical features in these skeletons, defects in the texture are identified. A complete review and taxonomy of texture defect detection schemes are discussed in [47] and [48] (a recent survey on automated visual inspection by Newman and Jain).

3.2. System Description

Any machine vision system whether this attempts to accomplish recognition, or identification , segmentation or classification tasks very generally can be thought to consist of two blocks. The first block is the so called feature extraction part. This is the place where data is transformed from higher dimensional space into lower dimensional form suitable for subsequent processing. Feature extraction is the most important part since the overall performance of a system primarily depends on the performance of this section. The second part, involves some kind of decision based on the data obtained in feature extraction phase. In recognition and identification, this is the block that makes matching against data gathered in advance and generates a decision whether the object under concern is among those known a priori. In classification the decision generated involves grouping of the data into classes under certain similarity measure. If the number or characteristics of classes are supplied beforehand this is called supervised classification. Thus, a defect detection system will be made up of those two blocks we mentioned above.

In this work, we mostly deal with the first block. We use different methods to extract features to detect defected regions in textured images. Before discussing each method separately here in below we describe, briefly, the general structure of our defect detection system and outline the common part for each method.

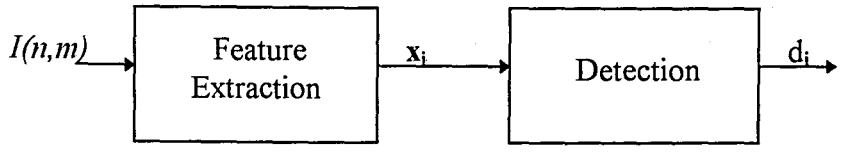

FIGURE 3.1. Defect detection system block diagram

Raw images $I(n,m)$ of size 256x256 acquired by a CCD camera are fed through the feature extractor as seen in Figure 3.1. Feature vectors are calculated within local nonoverlapping subwindows (S_i) of size NxN. The choice of subwindow size depends mainly on two factors: 1) how localized the defects are; and 2) for a nondefective sample how representative of the texture is the data in a window of such size [44]. Experiments we carried have shown that for the textures in our database size of 32x32 was the best selection (see Figure 3.2). Thus, each feature vector ($\mathbf{x}_i$) represents a certain distinct region of image $I(n,m)$.

The second block in Figure 3.1 named "detector" is a sort of classifier utilizing mahalanobis distance measure to assign each feature vector (i.e., each sub-region of the image) a label (class) as defective or nondefective. Formally, the classification is performed as follow:

A. *Learning phase*

1) Given k samples (subwindows) of defect free fabric images calculate feature vectors $\mathbf{s}_j$ for each sample ($1 \le j \le k$) using the feature extraction scheme that is to be used by the classifier.
2) Compute mean vector $\mathbf{m}$ and covariance matrix C for the feature vectors $\mathbf{s}_i$.

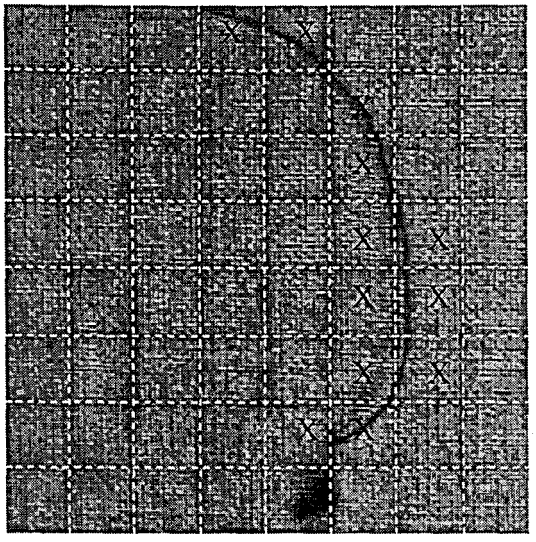

FIGURE 3.2. A defective textile fabric image and its partitioning. 'X' denotes defective subwindows as labeled by a quality inspector.

B. *Classification phase*

1) Divide a fabric image into nonoverlapping subwindows S_i and calculate features $\mathbf{x}_i$ for each subwindow.
2) Compute the mahalanobis distance d_i between each feature vector $\mathbf{x}_i$ and $\mathbf{m}$

$$d_i = (\mathbf{x}_i - \mathbf{m})^T C^{-1} (\mathbf{x}_i - \mathbf{m}) \qquad (3.1)$$

where $\mathbf{m}$ and C are mean vector and covariance matrix determined in the learning phase.

3) Classify a subwindow S_i for which d_i exceeds a threshold value (α) as defective else identify it as nondefective. i.e.,

$$S_i = \begin{cases} \text{defective} & \textit{if} \quad d_i > \alpha \\ \text{nondefective} & \textit{otherwise} \end{cases}$$

The threshold value is determined by the formula

$$\alpha = D_m + \eta\,(D_q - D_m)\,. \qquad (3.2)$$

D_m is the sample median of the order statistics D_i (distances d_i arranged in ascending order). For an 256x256 sized image partitioned into subwindows of size 32x32 D_m and D_q are given by: $D_m = (D_{32} + D_{33})\,/\,2$ and $D_q = (D_{48} + D_{49})\,/\,2$ respectively. η is a constant determined experimentally.

3.3. Pyramid Structured Wavelet Transform

Wavelets were shown [34] to form a complete basis for the representation of images in multi-resolution. Any signal can be decomposed into multiple frequency bands using a single set of filter coefficients. Furthermore wavelet transforms have good spatial/spatial-frequency localization. Directional information is inherent in wavelet coefficients. Namely the LH, HL and HH bands contain details in horizontal, vertical and diagonal directions respectively. Wavelet transform analysis facilitates inspection of spatial/spatial-frequency contents of a signal in a unified framework. All these properties constitute the background for their use in texture analysis.

In pyramid structured wavelet transform (PSWT), decomposition in each scale is carried throughout the low-low band whereas in tree-structured wavelet transform, decomposition can be applied into any band (Figure 3.3). Chang and Kuo [20] used irregular tree structure to represent textures. For textures with their energies concentrated in the middle frequencies this approach is reasonable. But when defect detection is concerned, this, most of the time due to the low-pass nature of textures reduces to the case of regular wavelet transform (i.e., pyramid structured wavelet transform). Our motivation in choosing pyramid structured wavelet transform can be explained by this observation.

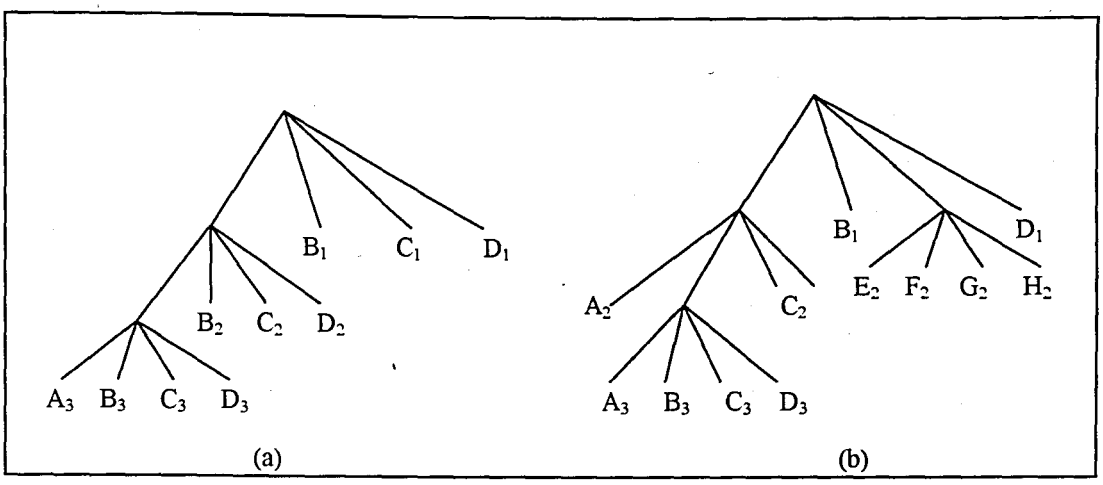

FIGURE 3.3. Pyramid-structured (a) and tree-structured (b) wavelet decomposition. (Branches from left to right indicate LL, LH, HL and HH frequency bands.)

3.3.1. The Algorithm

The feature extraction algorithm for texture defect detection with pyramid-structured wavelet transform is as follows:

i- Given a textured image $I(n,m)$ divide it into nonoverlapping sub-windows S_i of size 32x32. For image size 256x256 $1 \le i \le 64$.

ii- Decompose subimage S_i using 2-level pyramid-structured wavelet transform.

iii- Calculate the energy $e_{i,j}$ of the decomposed subimage (children node) as:

$$e_{i,j} = \frac{1}{N_j^2} \sum_n \sum_m \left| S_{i,j}(n,m) \right| \qquad (3.3)$$

where $N_j = 8$ for $0 \le j \le 3$ and

$N_j = 16$ for $4 \le j \le 6$.

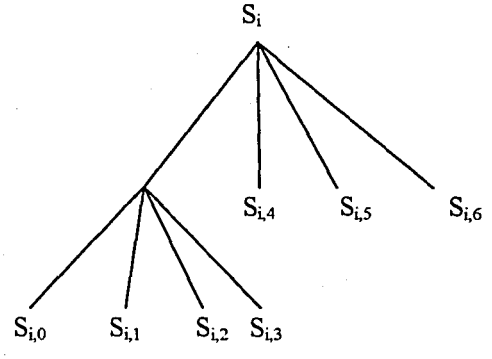

iv- Construct feature vector for subimage S_i as :

$$\mathbf{x}_i = [e_{i,0}\ e_{i,1}\ e_{i,2}\ \cdots\ e_{i,6}]^T.$$

v- Repeat steps (ii) to (iv) for all i.

3.3.2. Implementation and Results

Implementation of the algorithm is performed on a database consisting of 36 real fabric images obtained from the job site. Each image is of size 256x256. Seventeen of those images are defect free and the remaining 19 each contains defects of different type (class). A complete list of those images are provided in Appendix-B. Sixteen of the defect free images form the training set. The test set contains 19 defective and one defect-free image. Therefore total number of subwindows in the training and test sets are 1024 and 1280 respectively. The total number of subwindows labeled by a trained quality inspector as defective is 140.

Same feature extraction scheme is used in both training and test phases. Classification is done as described in section (3.2). During feature extraction decomposition is performed using Battle-Lemarie filter coefficients. For energy calculation we use l_1 -norm (Eq. 3.3). The gain in the computations by using l_1 -norm instead of l_2 -norm is in the order of the image data. Moreover, final results does not change much with the form of energy computation. Thus, our choice is fair. In the Table below, we provide the detection rates for each defect class (type) and the overall performance of the algorithm for our database.

TABLE 3.1. Performance of the PSWT based defect detection algorithm

Defect Class	Detection Rate (%)
dc1	89.06
dc2	87.50
dc3	85.94
dc4	93.75
dc5	79.69
dc6	81.25
dc7	90.63
dc8	92.19
dc9	92.19
dc10	87.50
dc11	89.06
dc12	85.94
dc13	90.63
dc14	87.50
dc15	84.38
dc16	92.19
dc17	87.50
dc18	90.66
dc19	82.81
Average	88.98

The constant η which maximized the detection rates for most of the defect types except few was 9.5. System can be tuned to individual defects by appropriate selection of constant η. This is demonstrated in Figure 3.4 where we plot the detection rates for average η (η_{avrg}) and η tuned for each defect type individually (i.e., η optimum per defect η_{opt}) .

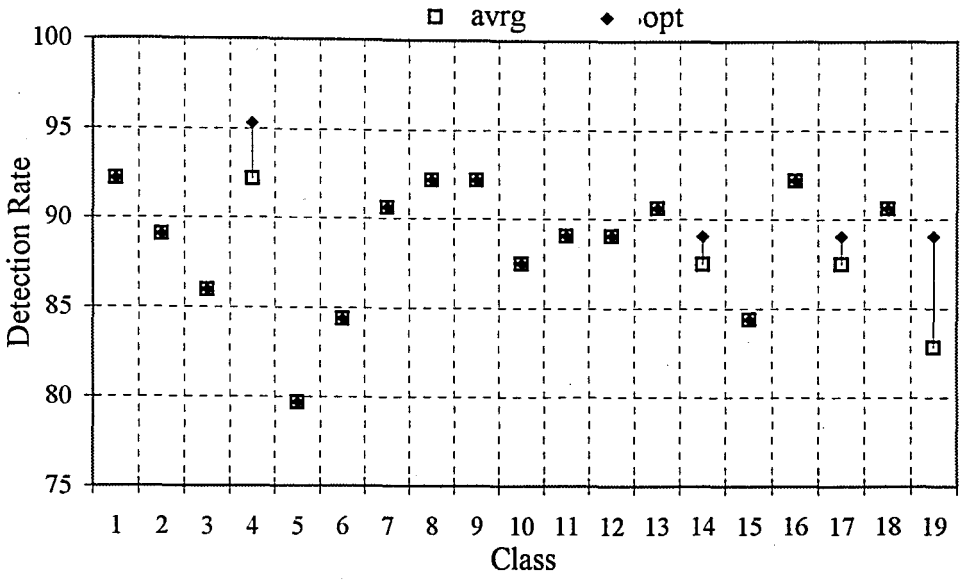

FIGURE 3.4. Average and best achievable detection rates using PSWT.

To provide a better evaluation of the detection capacity of the algorithm, in the following Figures, we give the false alarm rate versus correct detection rate plots for the whole database and individual defect types separately. We call these plots system operating curve (SOC). Depending on the costs of false alarm and miss for the process one can select the optimum operating point on these curves for the system.

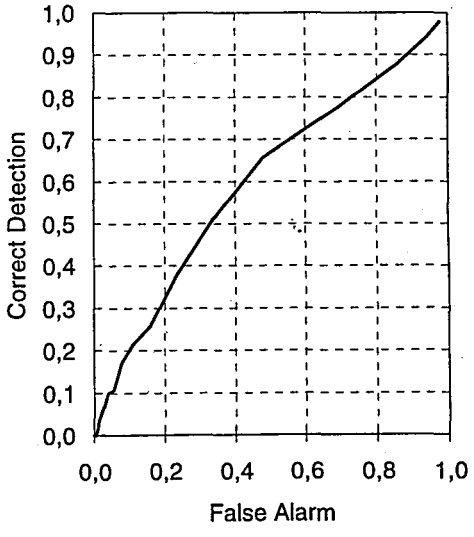

FIGURE 3.5. Average SOC curve for PSWT based system.

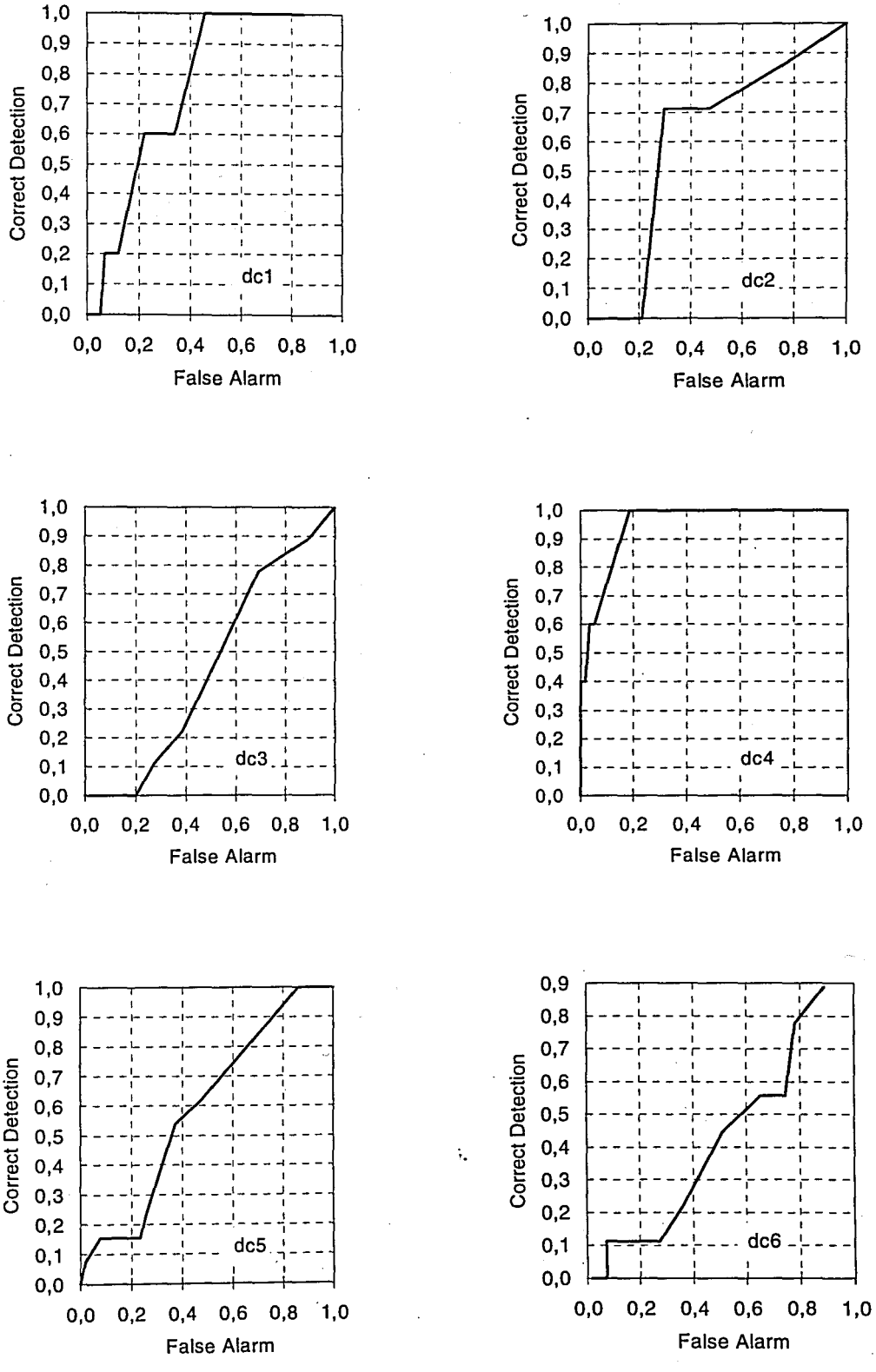

FIGURE 3.6. SOC curves for PSWT based system under each defect type.

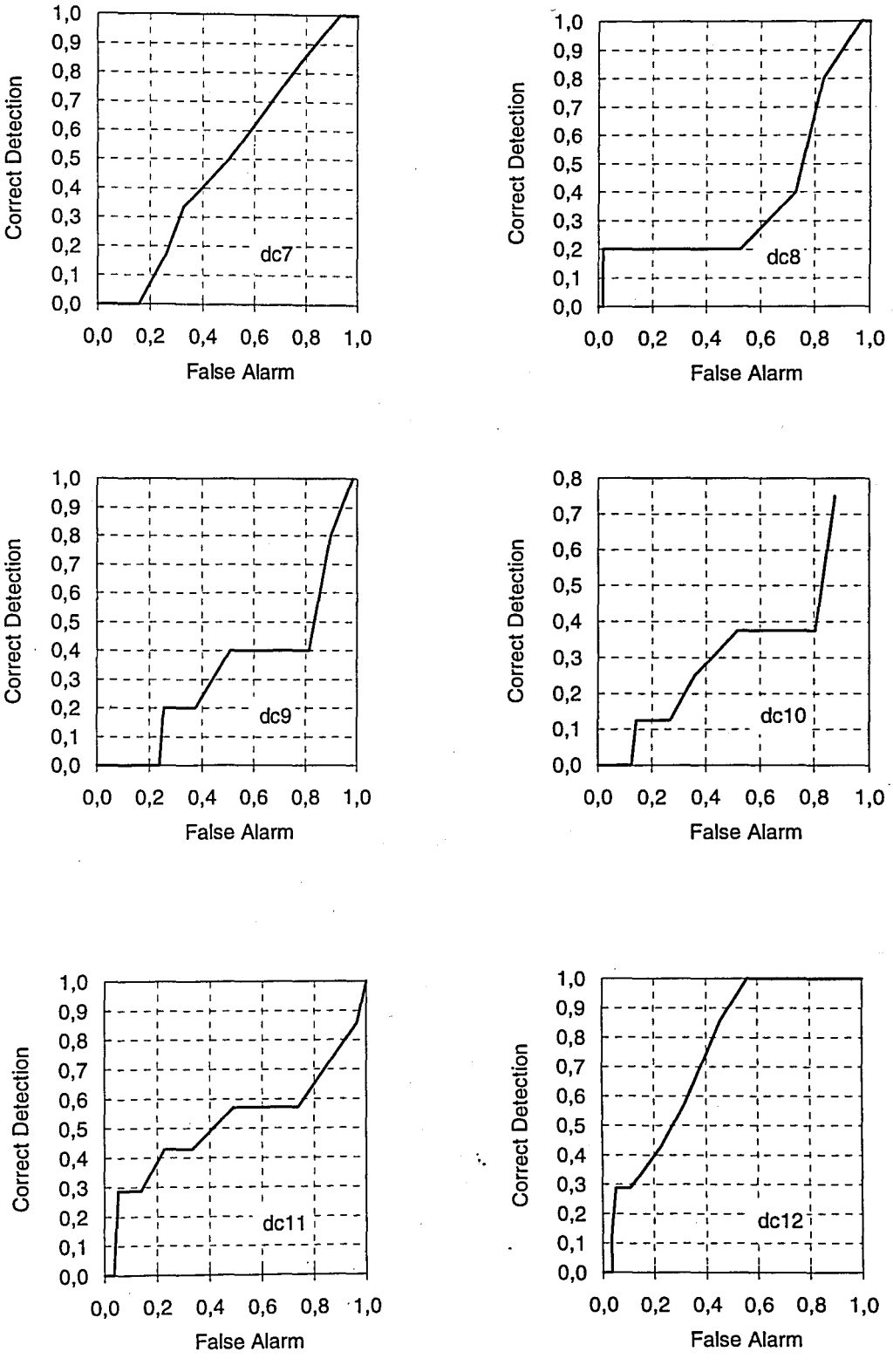

FIGURE 3.6. (continued)

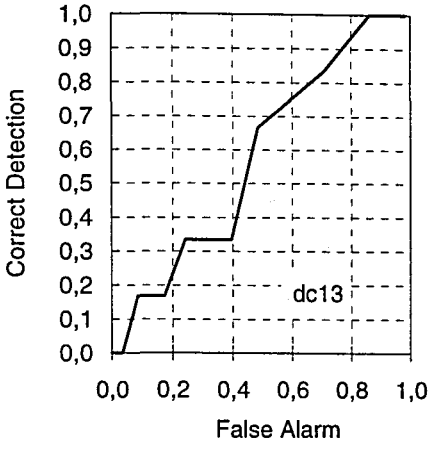

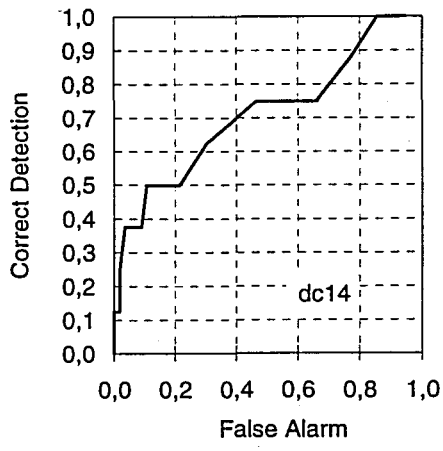

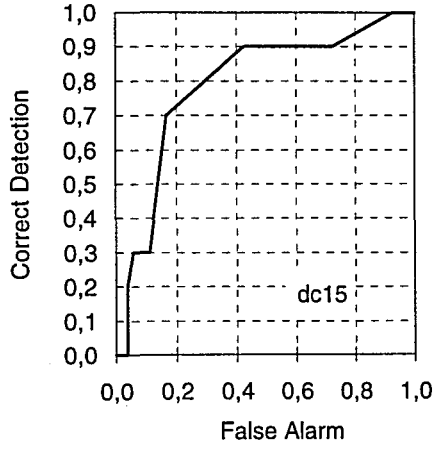

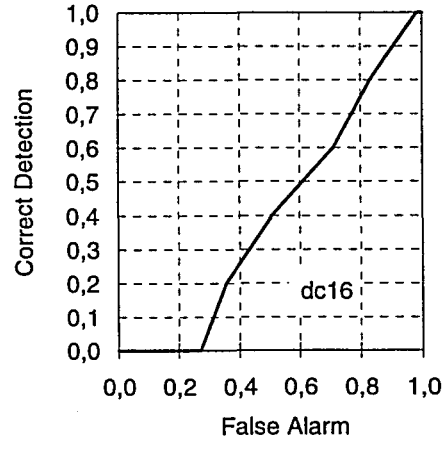

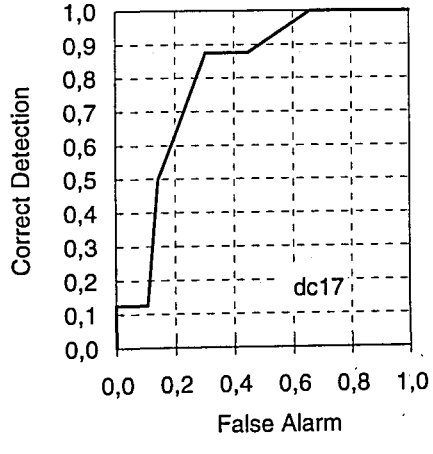

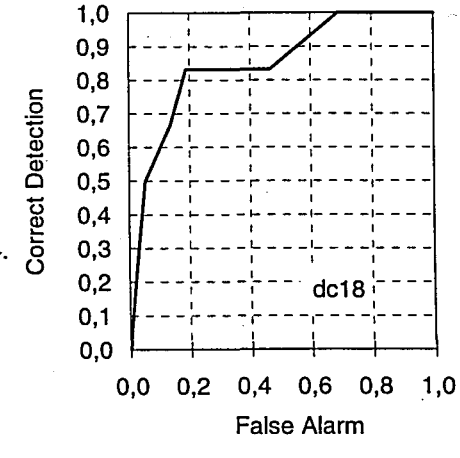

FIGURE 3.6. (continued)

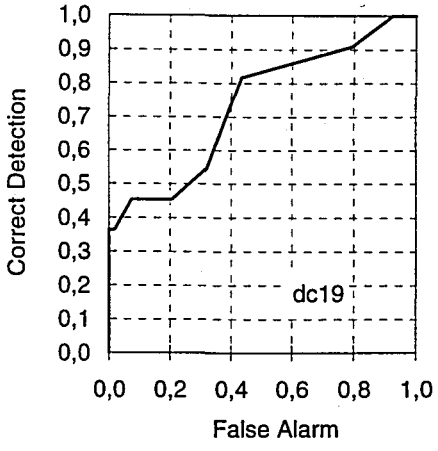

FIGURE 3.6. (continued)

3.4. Wavelet Packet Signatures

Decomposing images with PSWT or using wavelet packet (WP) bases, as we already discussed, does not differ much. Both can be implemented with a filter-bank by using same coefficients. The only difference is in building the tree seen in Figure 3.3. In WP expansion, the decomposition is carried through all branches of the tree whereas in PSWT only the leftmost branch (low-low band) is successively decomposed. Each node corresponds to the component of the signal along a basis. WP expansion is also closely related to subband decomposition. For example, outputs of 16-band decomposition of an image coincide with the leaf nodes in the 2-level WP expansion. The structure of the tree can be adapted to the signal characteristics by pruning the nodes that do not carry much information using certain measures. Such a scheme was used by Lee *et al.*[37] for surface defect classification and they called it adaptive wavelet packet (AWP) decomposition. Certainly, deriving the optimum tree structure is a subject of second interest. It can be considered once the appropriateness of the wavelet packet features to the problem at hand is asserted. In the following section, we list the algorithm for extracting features using wavelet packet expansion.

3.4.1. The Algorithm

For an image I $(n.m)$ the wavelet packet signatures (WPS) can be computed via the following steps:

i- Partition image I $(n.m)$ into nonoverlapping subwindows 32x32 S_i $(1 \le i \le 64)$.

ii- Apply 2-level wavelet packet expansion into each subwindow S_i .

iii-Compute energy $e_{i,j}$ of the decomposed subimage as :

$$e_{i,j} = \frac{1}{N_j^2} \sum_n \sum_m |S_{i,j}(n,m)| \tag{3.4}$$

where $N_j = 16$ for $1 \le j \le 4$ and $N_j = 8$ for $5 \le j \le 20$.

v- Construct feature vector for subimage S_i as :

$$\mathbf{x}_i = [e_{i,5} \;\; e_{i,6} \;\; e_{i,7} \;\; \cdots \;\; e_{i,20}]^T.$$

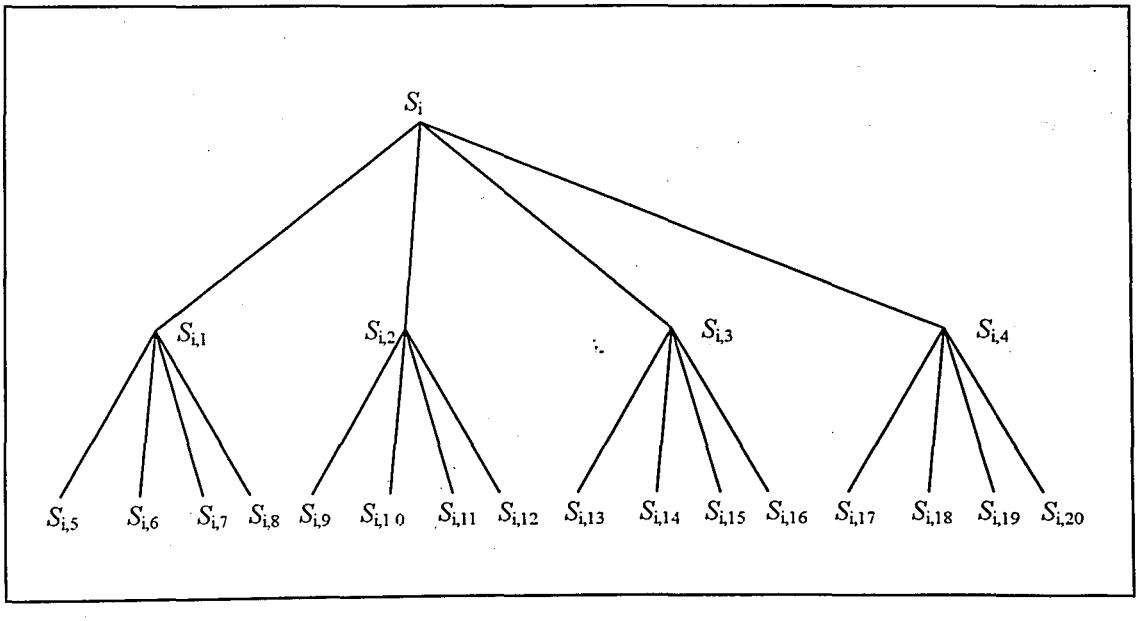

FIGURE 3.7. Wavelet Packet expansion of subimage S_i

3.4.2. Implementation and Results

Implementation is carried out on the same database and setup outlined in section (3.3.2). For the feature vector we selected the energy values of the outmost level that is the leaf nodes in the full expansion tree. Results are shown in the following Table and Figures.

TABLE 3.2. Performance of the WPS based defect detection algorithm

Defect Class	Detection Rate (%)
dc1	93.75
dc2	89.06
dc3	85.94
dc4	92.19
dc5	79.69
dc6	85.94
dc7	90.63
dc8	92.19
dc9	92.19
dc10	87.50
dc11	89.06
dc12	89.06
dc13	90.63
dc14	87.50
dc15	84.38
dc16	92.19
dc17	87.50
dc18	90.63
dc19	82.81
Average	89.14

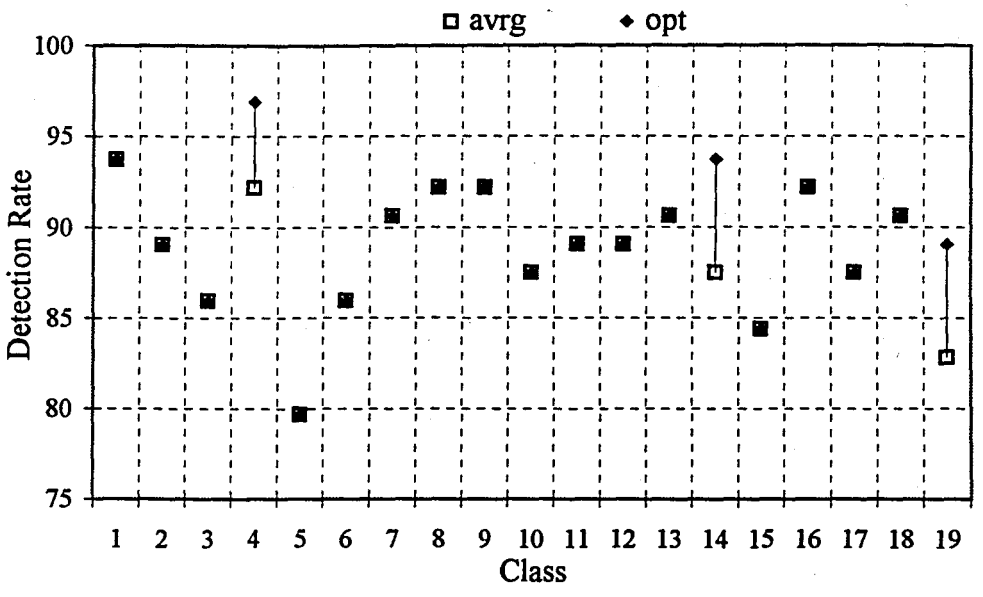

FIGURE 3.8. Average and best achievable detection rates using WPS

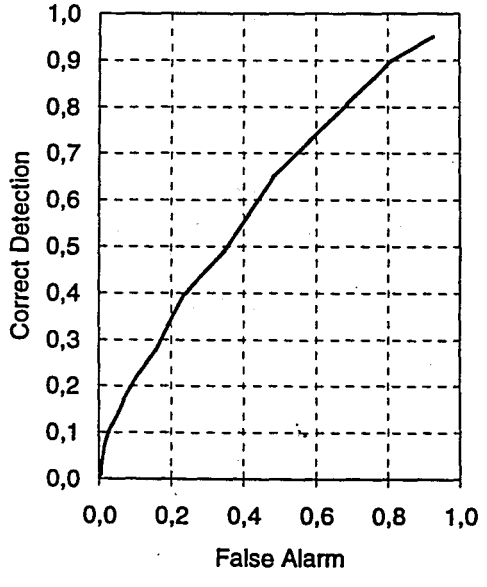

FIGURE 3.9. Average SOC curve for WPS based system.

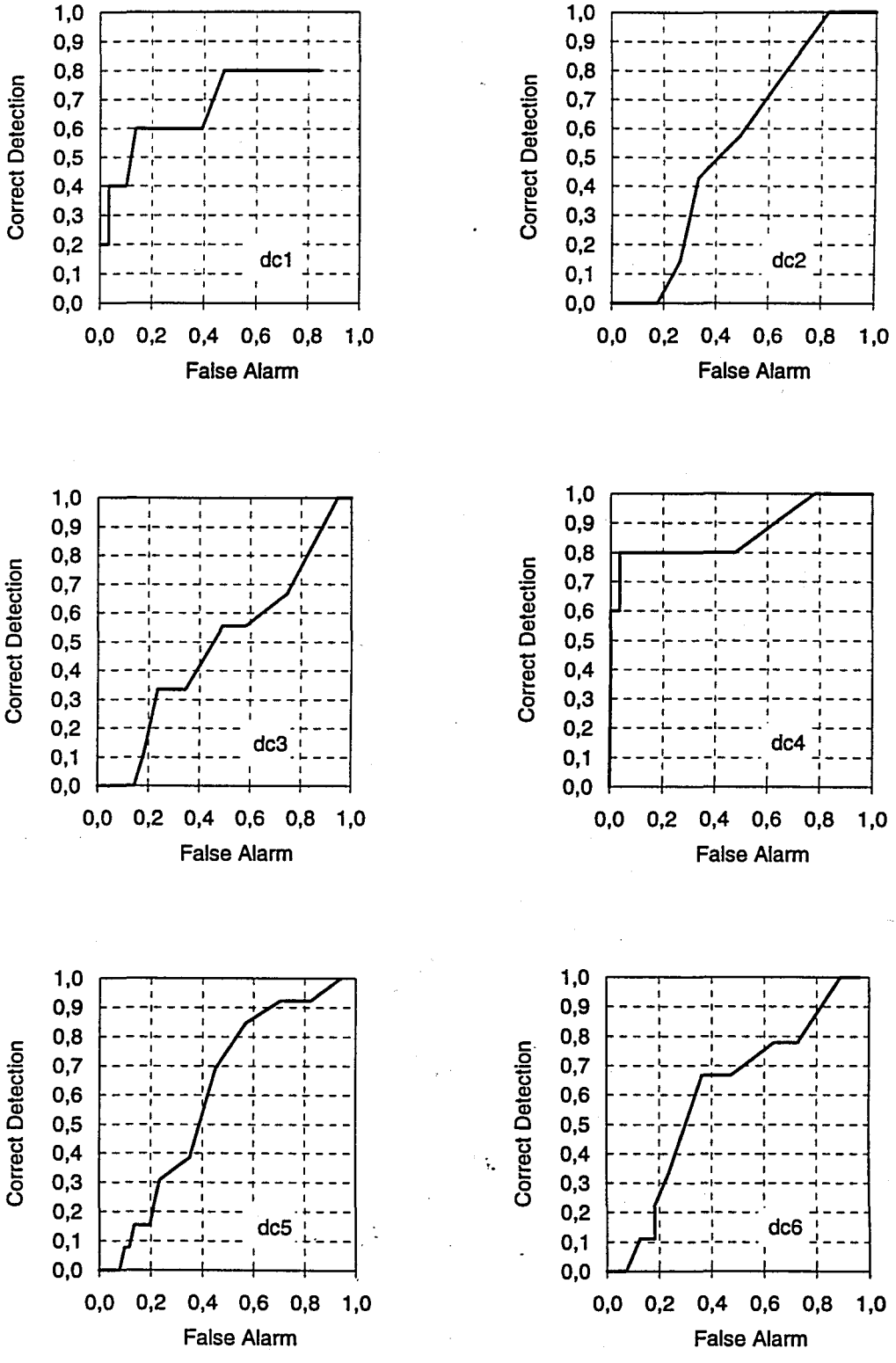

FIGURE 3.10. SOC curves for WPS based system under each defect type.

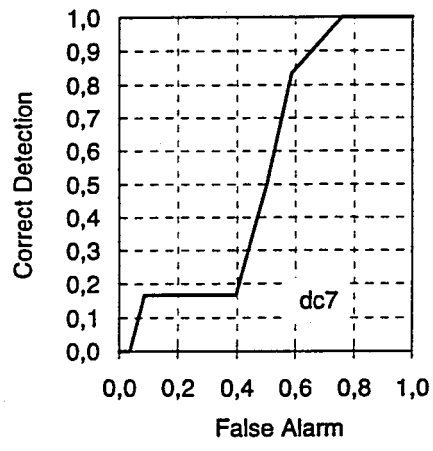

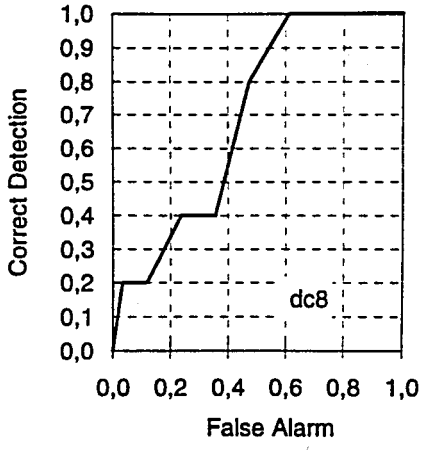

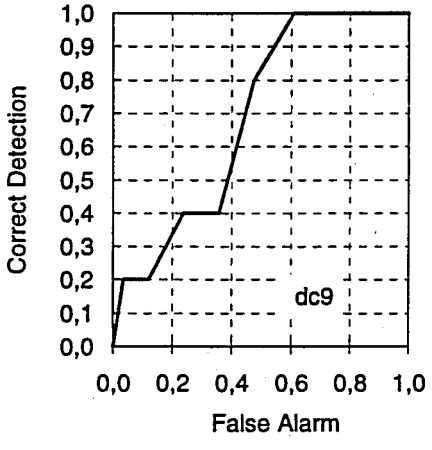

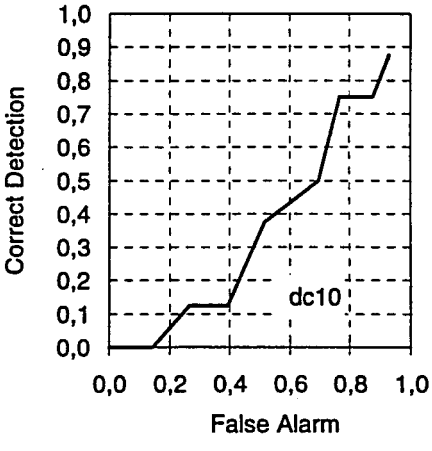

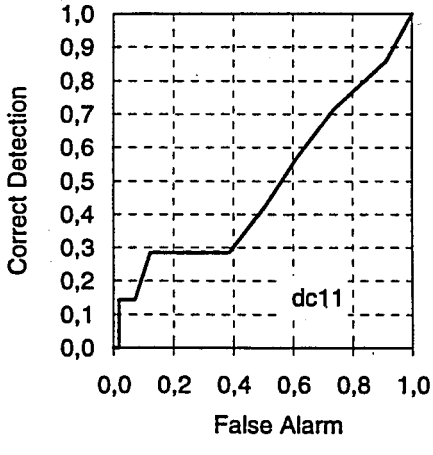

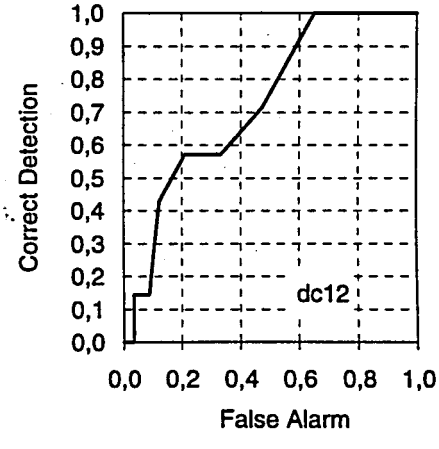

FIGURE 3.10. (continued)

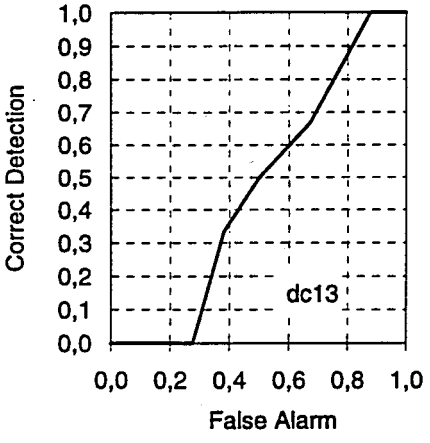

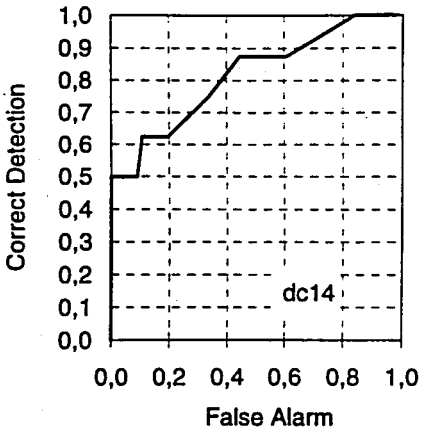

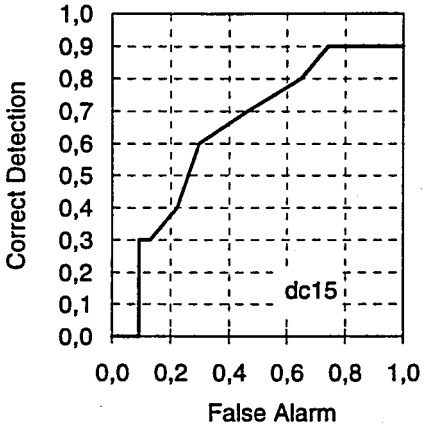

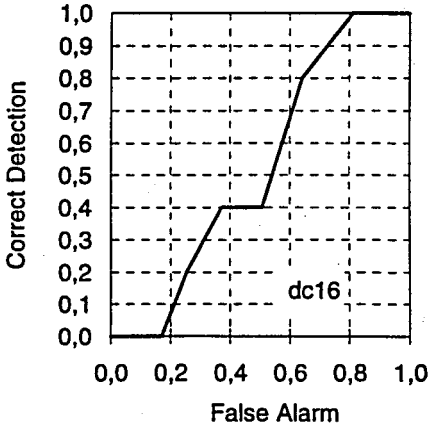

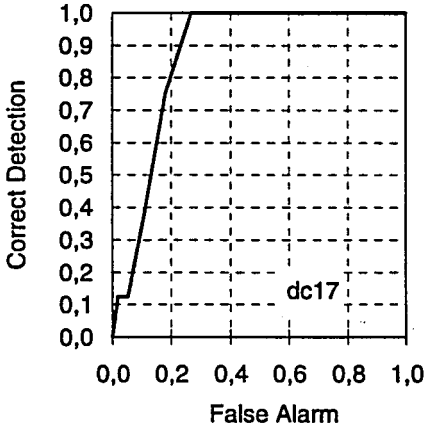

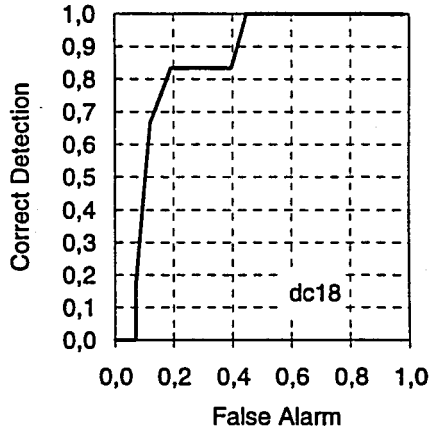

FIGURE 3.10. (continued)

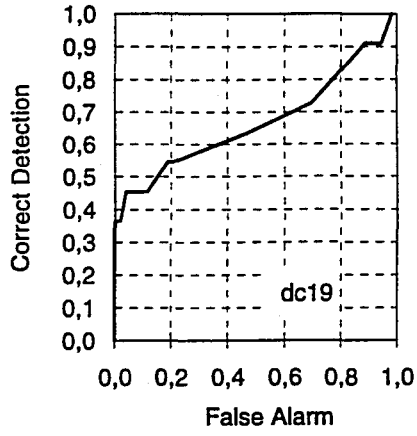

FIGURE 3.10. (continued)

3.5. Multichannel Spatial Filtering

In chapter two while defining the texture analysis tools, we have seen Gabor functions to possess important properties facilitating texture analysis applications. Especially the optimal spatial/spatial-frequency localization they have and the degree of freedom they offer in designing filters for a particular purpose are two main criteria which made us to consider their use for texture defect detection problem. They were successfully used by a number of researchers for segmenting and classifying textured images [21-27]. The texture defect detection, in its nature, is a problem in between. One has to locate (in the strict sense) or (at least) inform about the existence of regions in an image that visually appear to differ from the rest.

It is experimentally verified that early visual processing mechanism in the striate cortex of mammals make use of spatial-frequency information. Hence modeling that will incorporate frequency measure will serve for mimicking the human visual system in discriminating and detecting defected regions in a textured image. Although the entire visual

system can not be simplified to a linear mathematical model, it is believed that using frequency information is more appropriate than features derived from the first or second order statistics of the gray levels bearing certain shortcomings as conjectured by Julesz [28].

3.5.1. The Algorithm

Feature extraction algorithm for the gabor filtering based system is as follows:

i- Given an image $I(n,m)$ decompose it into multiple frequency channels using a bank of gabor filters $\{h_i(n,m)\,;\, 1 \le i \le L\}$.

$$I_i(n,m) = h_i(n,m) * I(n,m)$$

ii- Divide output image of each channel $I_i(n,m)$ into 32x32 sized nonoverlapping subimages $I_{i,k}(n,m)$

iii- Calculate energy for each subimage $I_{i,k}(n,m)$ as :

$$e_{i,k} = \frac{1}{N^2} \sum_n \sum_m \left| I_{i,k}(n,m) \right| \qquad (3.5)$$

where $N = 32$.

iv- Construct feature vector for subimage k as :

$$\mathbf{x}_k = [e_{1,k}\ e_{2,k}\ e_{3,k}\ \cdots\ e_{L,k}]^T.$$

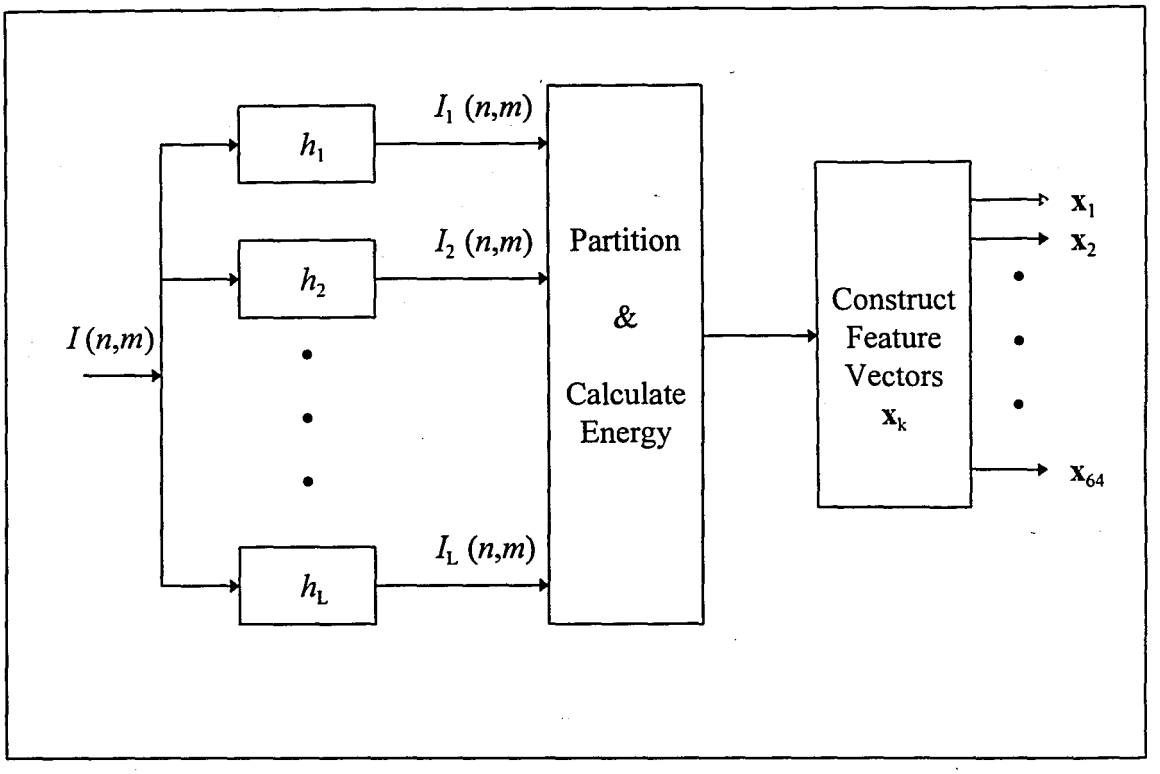

FIGURE 3.11. Multichannel feature extraction

3.5.2 Implementation and Results

Experimental validation of the algorithm is performed using the same database and test setup described in section (3.3.2). Textured images are decomposed using 28 complex 2-D gabor filters tuned at seven radial frequencies (F) each one octave apart ($1\sqrt{2}, 2\sqrt{2}, 4\sqrt{2}, 8\sqrt{2}, 16\sqrt{2}, 32\sqrt{2}, 64\sqrt{2}$ cycles/image-width) and four orientations (0, 45, 90 and 135 degrees). Selection of radial bandwidth as one octave (B) was motivated by psychophysical findings which have shown this to be a good approximate for the cells in the early visual system of mammals [40],[49],[50]. Orientation bandwidth (Ω) was chosen to be 45 degrees. These 28 filters form a nearly orthogonal set and provide uniform coverage of the frequency plane. (for details see ref. [25]). For numerical implementation of filtering operation we used FFT algorithm.

Classification is done as outlined in section (3.2). The constant η (η_{avrg}) yielding maximum detection rate was determined to be 4.5. Results are summarized in Table 3.3. and Figures 3.13, 3.14, 3.15. Comparing with the PSWT based features and WPS, the improvement in the detection performance obtained by multichannel features is apparent. The advantage of this scheme is that it can serve as an initial step for a more general system (Figure 1.1) performing defect type classification in addition to detection of defects. Structure of such a system would be as follow. First, inspect fabrics for defects using the algorithm we presented in the previous section. Upon detection of defects switch to off-line mode and using available feature images obtained by Gabor filtering (Figure 3.12) segment the defective regions and using certain shape moments classify defects.

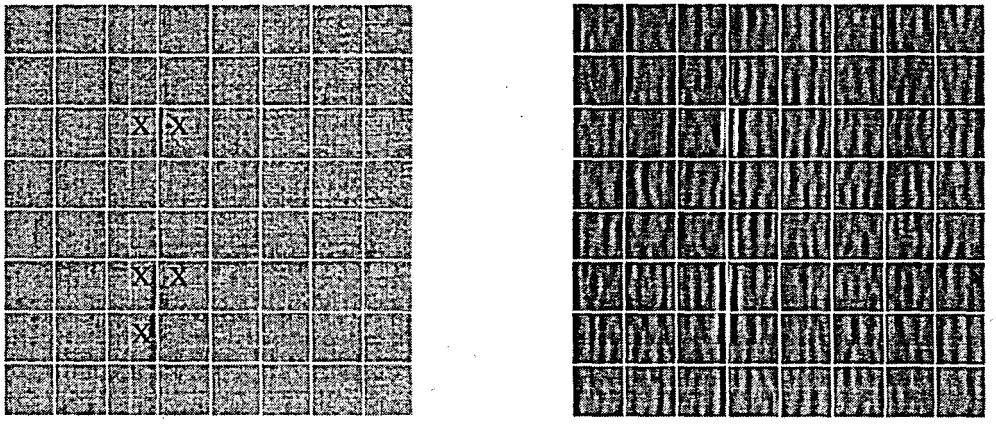

a b

FIGURE 3.12. (a) Defective fabric image 'dc1' and (b) the feature image obtained by Gabor filtering with filter parameters $(B,\Omega, F,\theta) = (1,\pi/4,32,0)$. 'X' shows defective blocks.

TABLE 3.3. Performance of the Gabor filtering based defect detection algorithm

Defect Class	Detection Rate (%)
dc1	96.88
dc2	89.06
dc3	90.63
dc4	95.31
dc5	87.50
dc6	89.06
dc7	89.06
dc8	92.19
dc9	92.19
dc10	85.94
dc11	87.50
dc12	98.44
dc13	92.19
dc14	90.63
dc15	89.06
dc16	98.44
dc17	100.00
dc18	96.88
dc19	84.38
Average	92.03

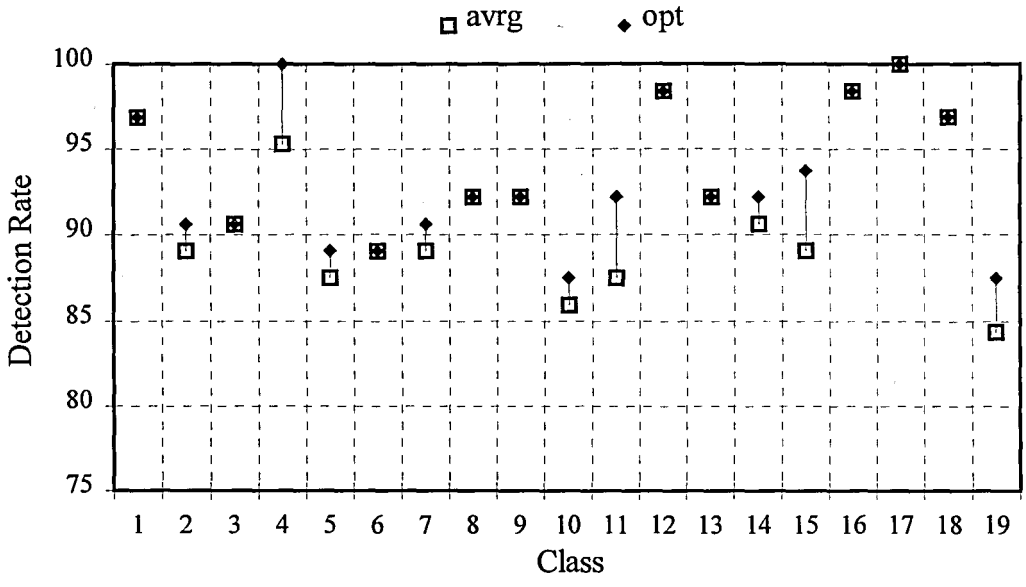

FIGURE 3.13. Average and best achievable detection rates using Gabor features.

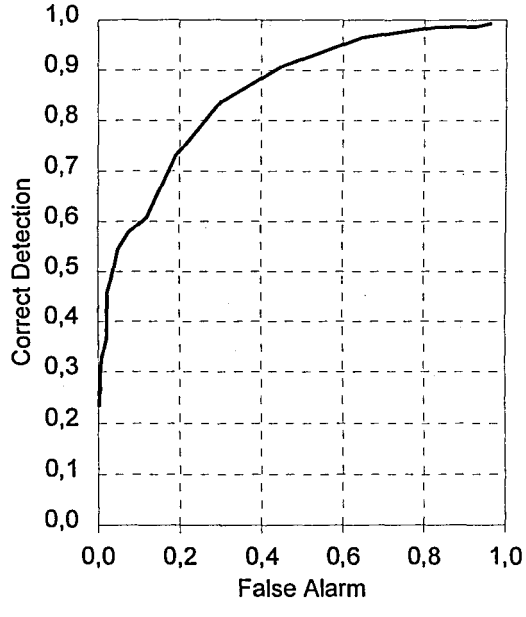

FIGURE 3.14. Average SOC curve for Gabor based system.

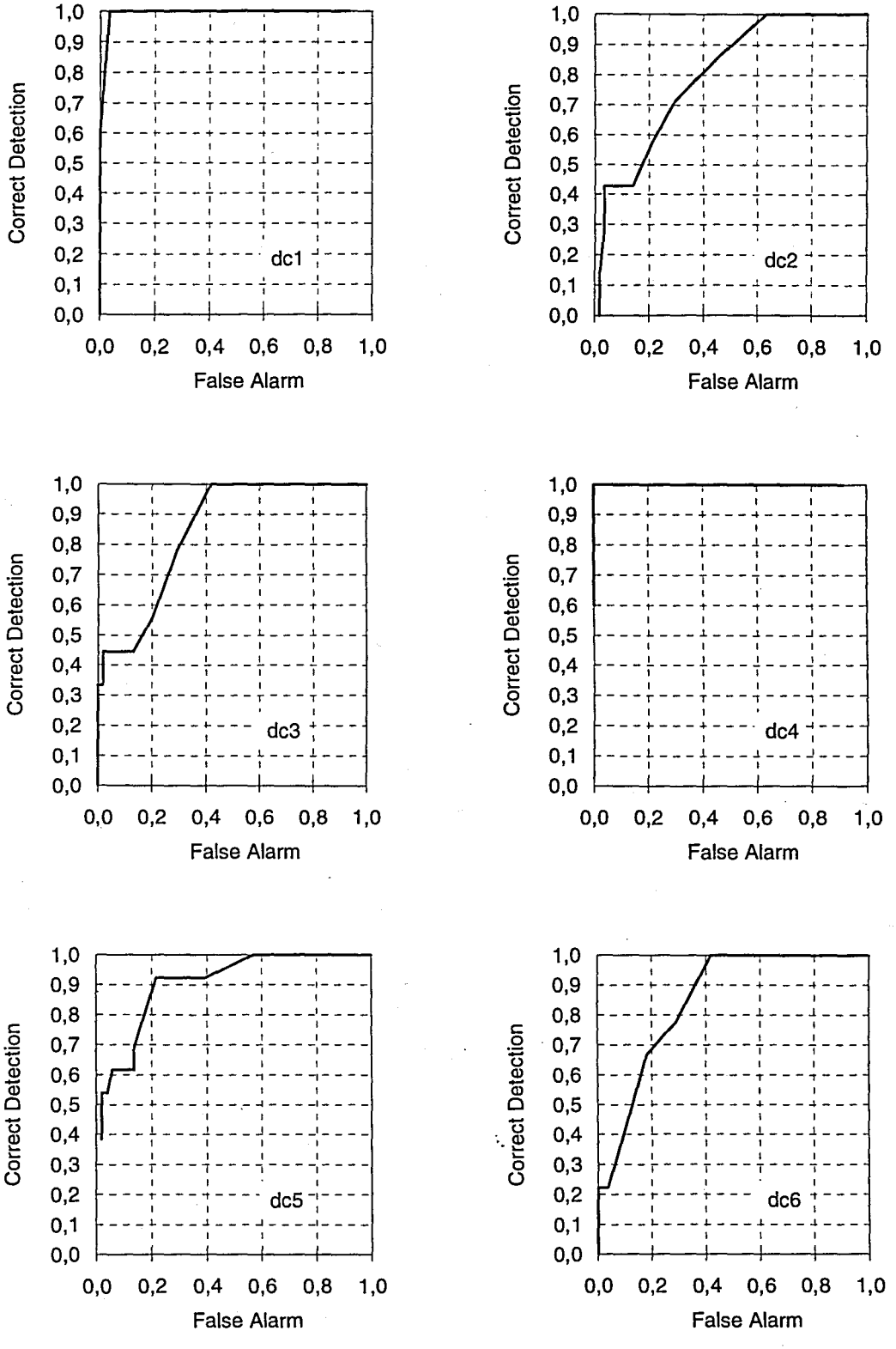

FIGURE 3.15. SOC curves for Gabor based system under each defect type.

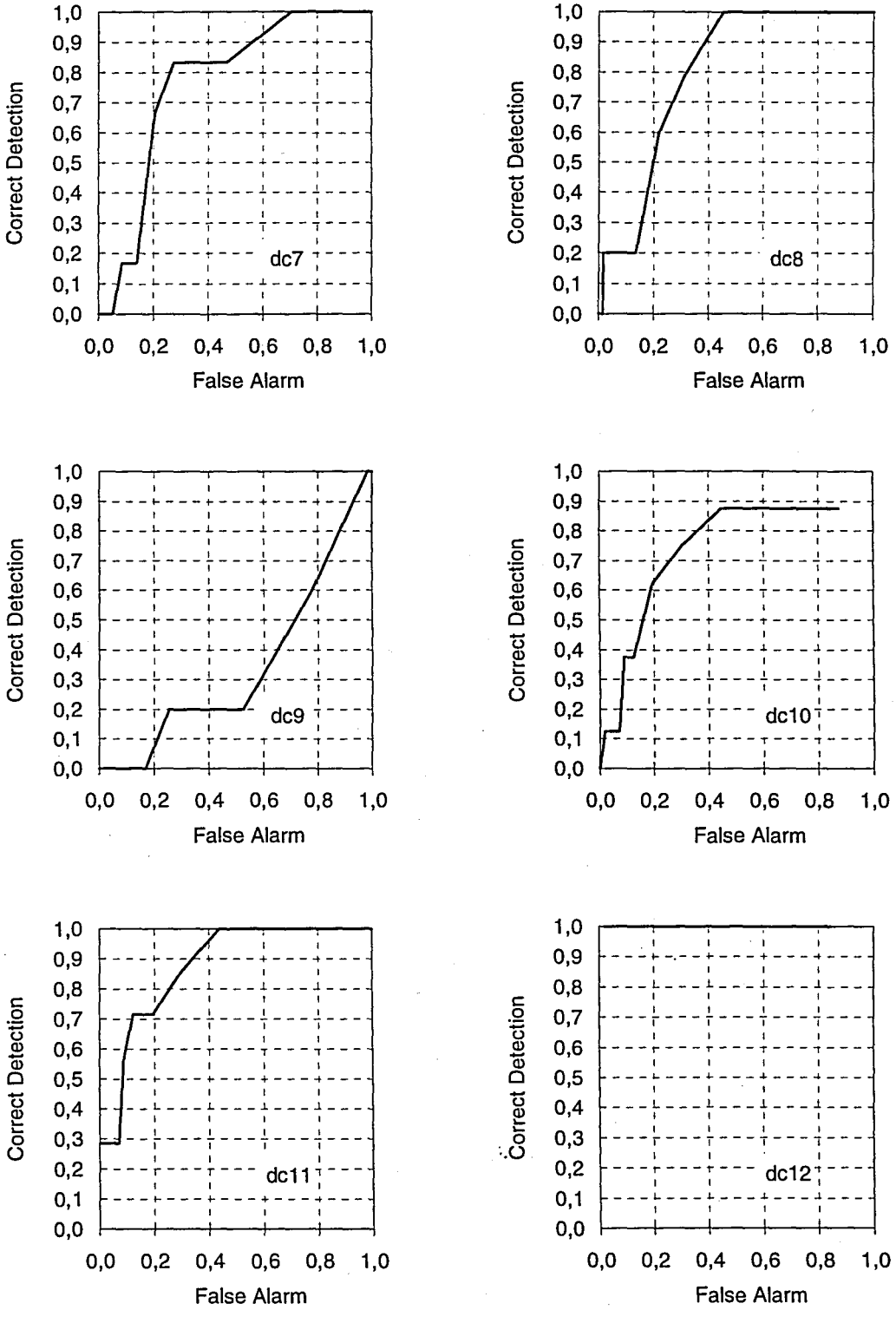

FIGURE 3.15. (continued)

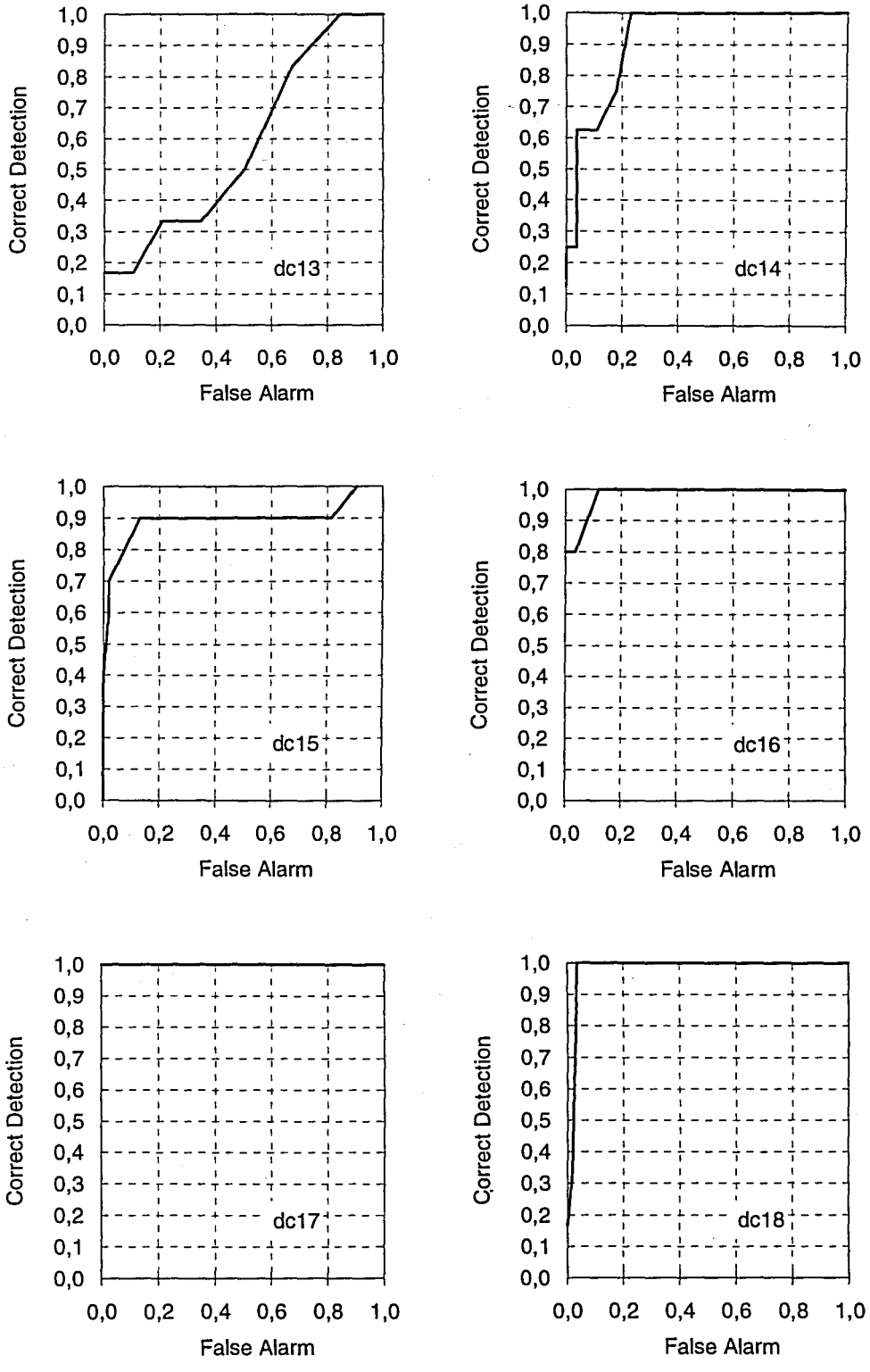

FIGURE 3.15. (continued)

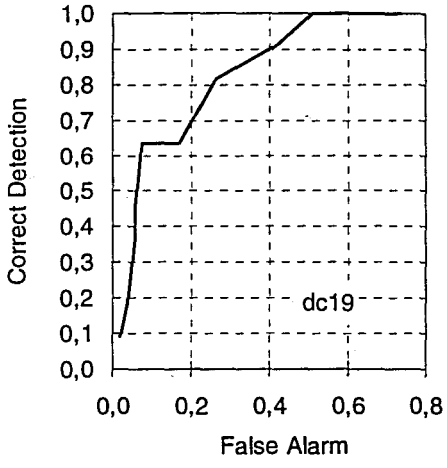

FIGURE 3.15. (continued)

3.6. Spatial Domain Co-occurrence Matrices

Co-occurrence matrices since their first usage by Julesz [28], were applied into several texture analysis problems. Performance of features computed from co-occurrence matrices has become a subject of debate. In some applications it was argued that co-occurrence features outperformed frequency and model based features [31],[32], while in others just the opposite. Our sole purpose of studying co-occurrence features here was not to introduce a new debate but to make better assessment of the wavelet transform based algorithms as compared to this well known method. Therefore, this part brings nothing new than application of co-occurrence features to our database. For the sake of completeness we give the algorithm in the section to follow.

3.6.2. The Algorithm

Given a textile fabric image $I(n,m)$:

i- Partition the image into nonoverlapping subwindows S_i each of size 32x32. For image size 256x256 : $1 \leq i \leq 64$

ii- Derive the co-occurrence matrices P_θ for d =1 (pixel separation distance) and angles $\theta = (0, \pi/4, \pi/2, 3\pi/4)$ radians.

iii-Calculate ENT, CON, ASM, IDM for each co-occurrence matrix as in equations (2.2)-(2.5).

iv-Compute mean μ_X and standard deviation σ_X for each feature of four angles.

v- Construct the feature vector as :

$$x_k = [\mu_{ENT}\ \sigma_{ENT}\ \mu_{CON}\ \sigma_{CON}\ \mu_{ASM}\ \sigma_{ASM}\ \mu_{IDM}\ \sigma_{IDM}]^T.$$

vi-Repeat steps (ii) to (v) for all i.

3.6.2. Implementation and Results

As it was previously mentioned, the application of all algorithms presented heretofore was carried on a database consisting of 36 real textile fabric images each of size 256x256 and 8-bits long. During the implementation, to keep the size of the co-occurrence matrices in a moderate level we quantized the raw images into 8 levels using uniform scalar quantizer. Such a reduction in the order of the co-occurrence matrices is vital if this algorithm is to operate in a real time system. Furthermore the degradation in the performance is insignificant when compared with the order of computational saving. Results obtained for 19 defect types and overall test set are summarized in Table 3.4. Figure 3.16 shows the best achievable detection rates and average detection rates per defect type. While the false alarm versus correct detection rate plots (i.e., SOC curves as

we called) are presented in Figures 3.17 and 3.18. Concluding, what can be addressed for the sake of comparison with the wavelet transform and gabor filtering based features is that performancewise co-occurrence features fall in between.

TABLE 3.4. Performance of the SDCM based defect detection algorithm

Defect Class	Detection Rate (%)
dc1	95.31
dc2	87.50
dc3	85.94
dc4	100.00
dc5	81.25
dc6	84.38
dc7	90.63
dc8	93.75
dc9	90.63
dc10	87.50
dc11	90.63
dc12	93.75
dc13	90.63
dc14	90.63
dc15	82.81
dc16	93.75
dc17	89.06
dc18	90.63
dc19	79.69
Average	89.92

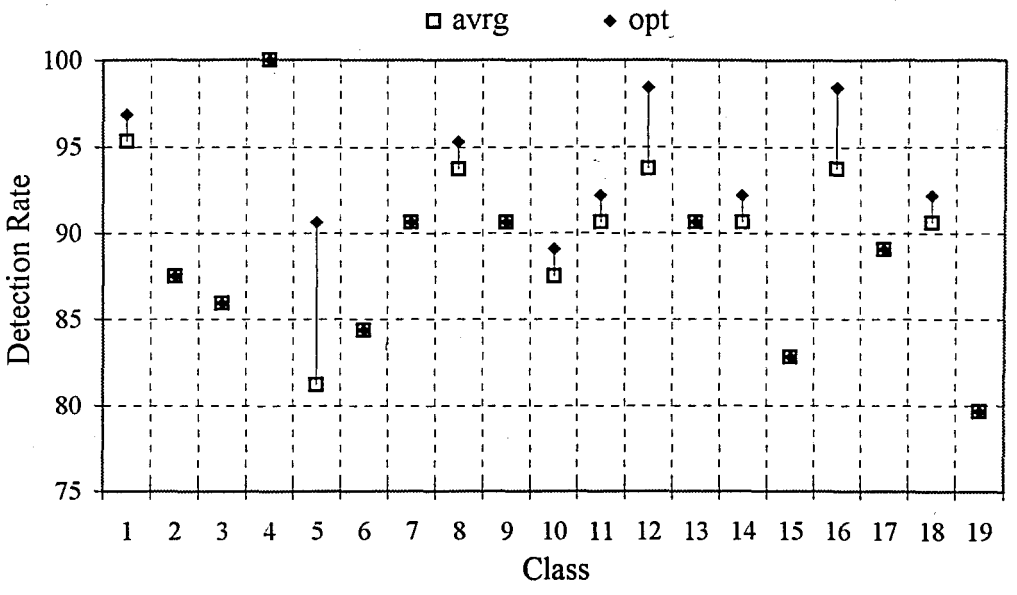

FIGURE 3.16. Average and best achievable detection rates using SDCM features.

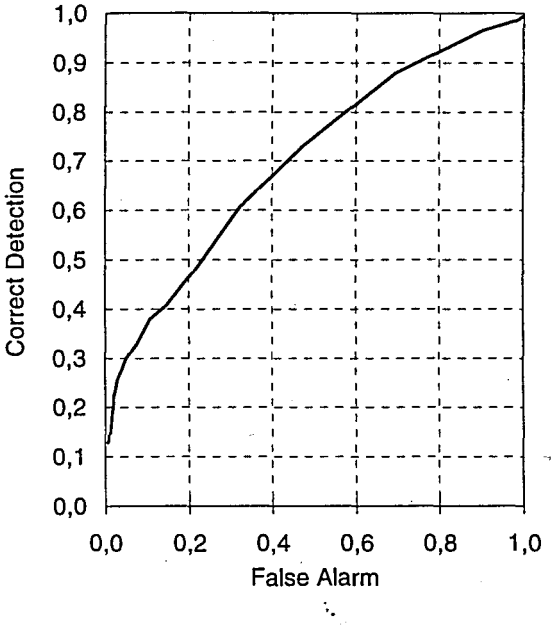

FIGURE 3.17. Average SOC curve for SDCM based system.

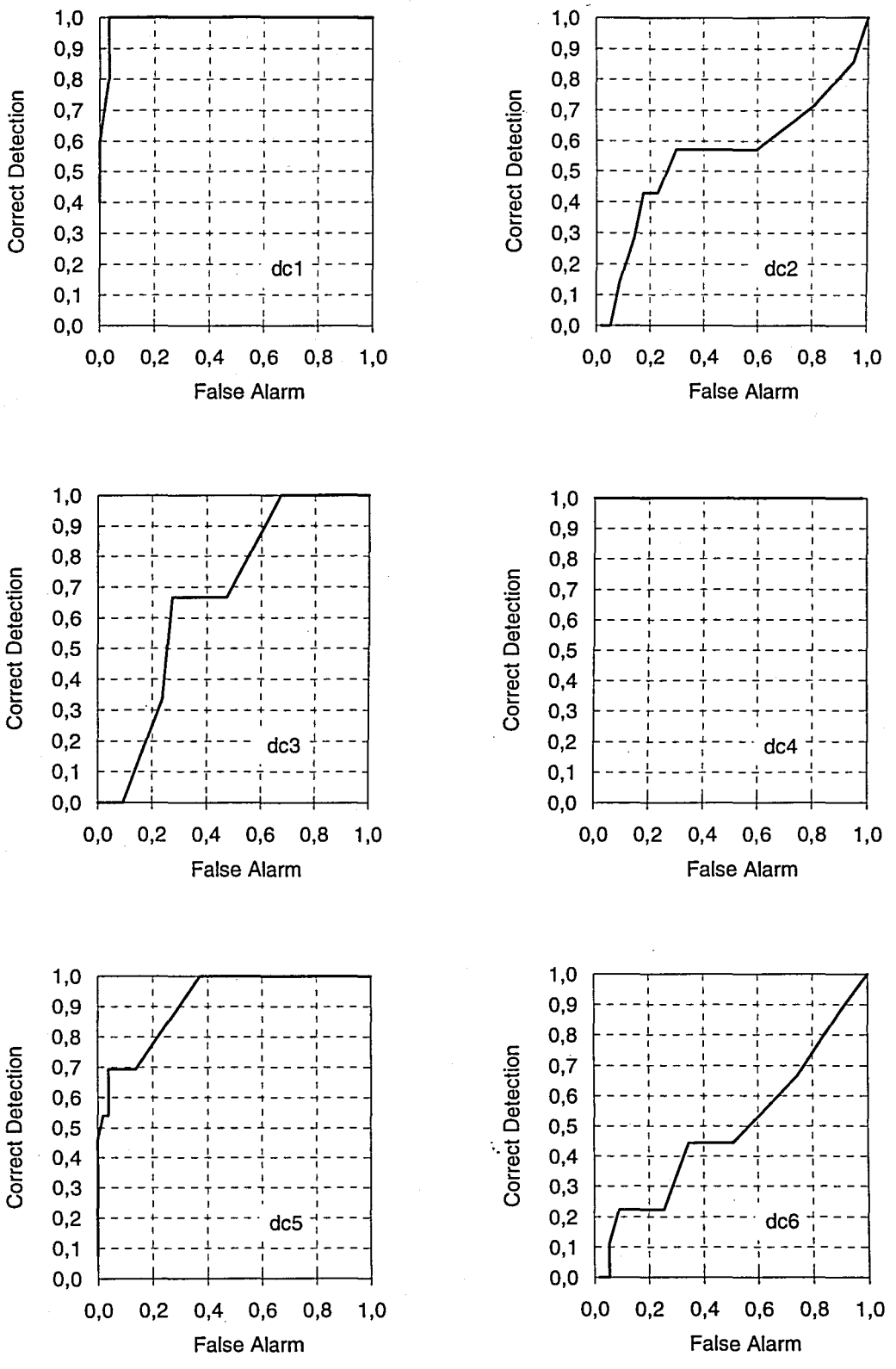

FIGURE 3.18. SOC curves for SDCM based system under each defect type.

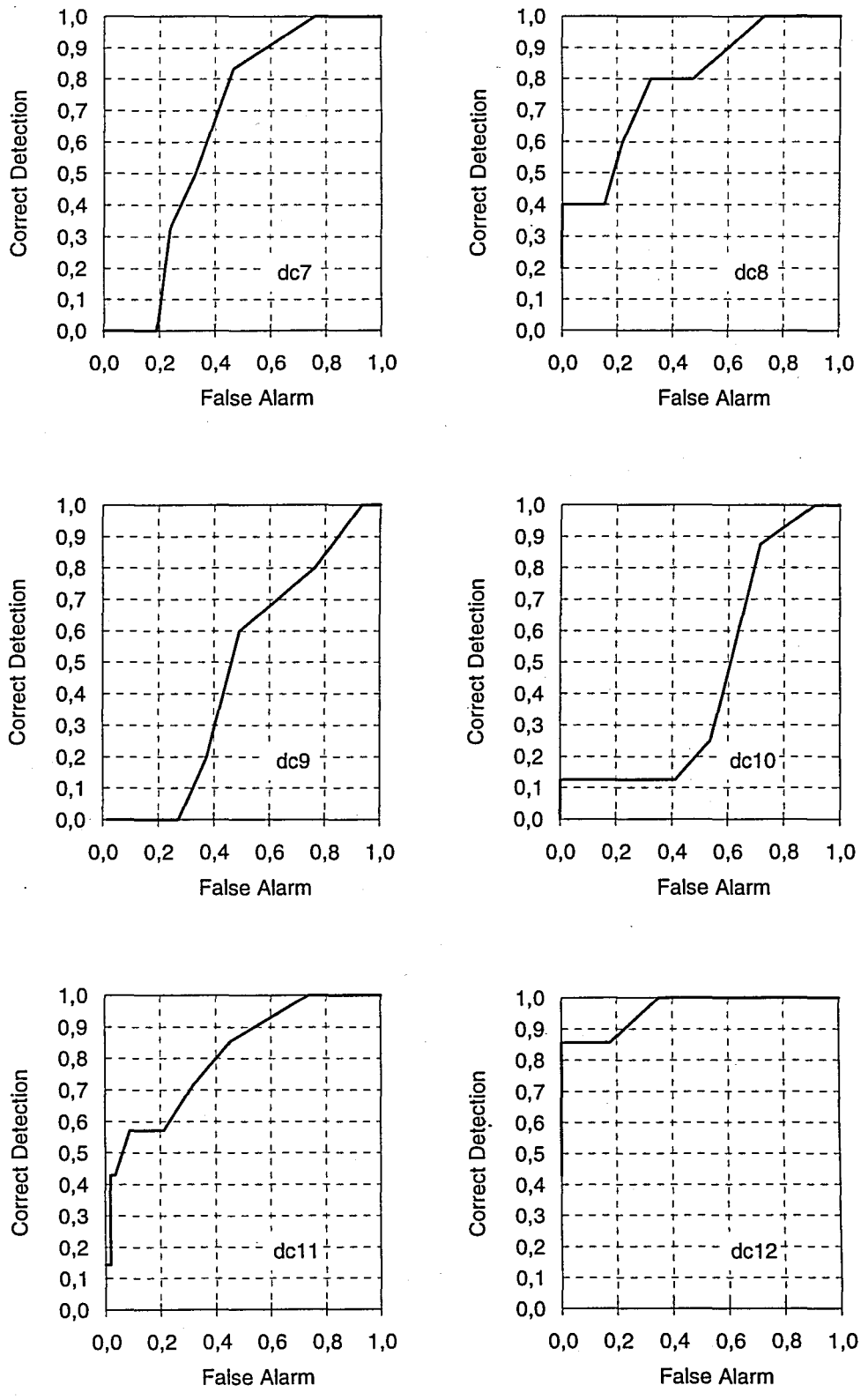

FIGURE 3.18. (continued)

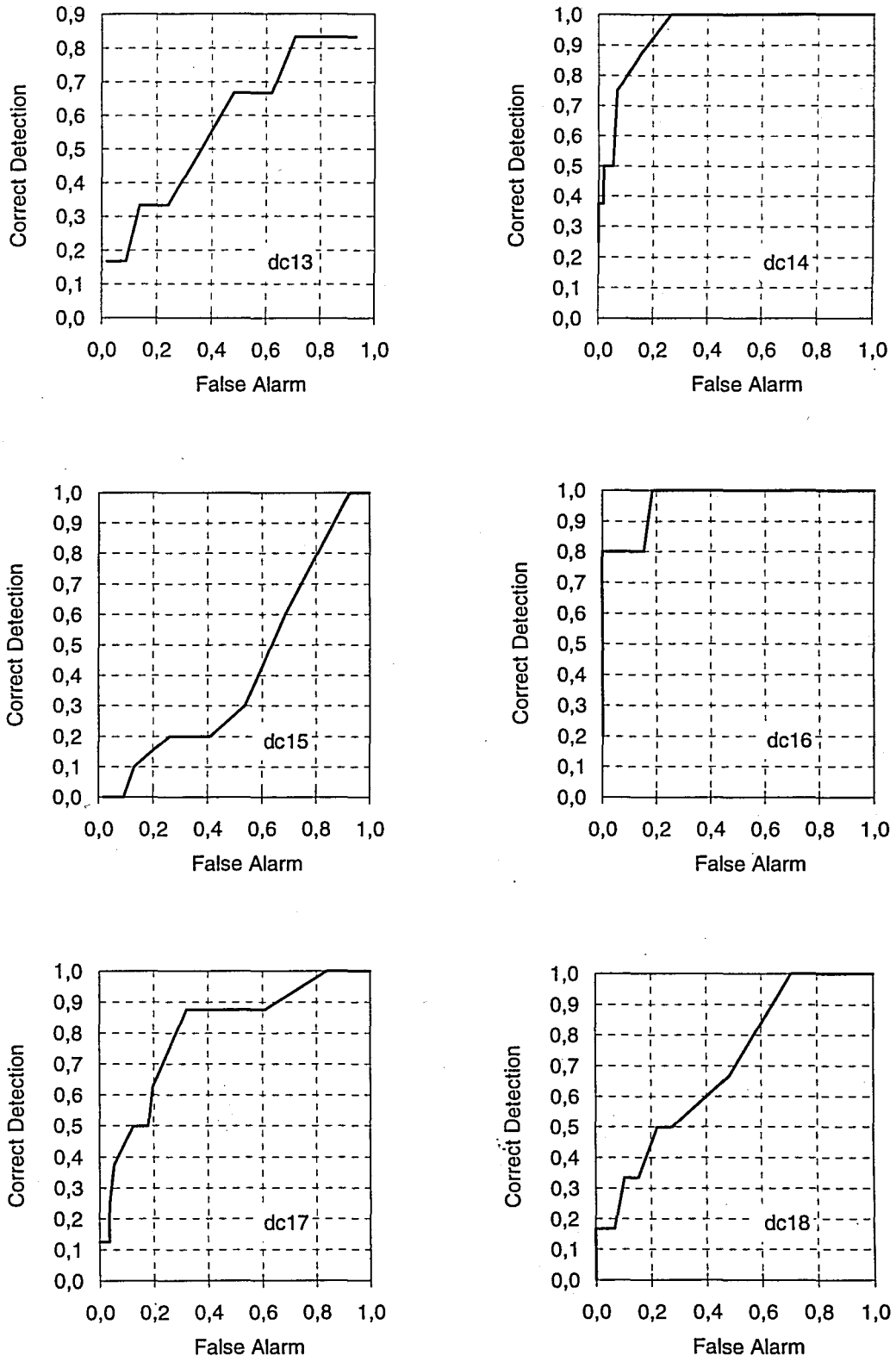

FIGURE 3.18. (continued)

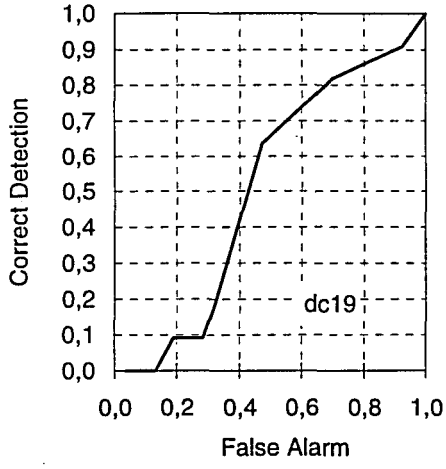

FIGURE 3.18. (continued)

3.7. A New Approach : Texture Defect Detection Using Subband Domain Features

Tests with wavelet transforms and co-occurrence features have shown two things. Lowpass characteristic of the textile images known by observation up to that moment were approved numerically with the examination of wavelet decomposed images. Energy contentment of the low-low band was around 60 per cent while high-high band had only the 5 per cent. Second co-occurrence features compared with wavelet transform features were more powerful in capturing defects.

These two observations made us to consider extracting co-occurrence features from subband images. Advantage of such an approach would have been twofold : First, dealing with smaller images would mean improvement in the computational efficiency since the calculation of co-occurrence matrices is directly proportional to the image data points (see Appendix A). Second, elimination of higher frequency bands which most of the time had a noise-like appearance and defects were barely noticeable if at all, and focusing on the lower resolution images would mean enhancement of defects relative to the background texture. Moreover discarding high frequency details which did not contribute for the detection of

defects visually, and concentrating on lower frequency bands carrying most of the information is in compliance with the theory since, as we have seen in the study of the Gabor filters, theory is based on the optimality of the human visual system and attempts to discover mathematical models to imitate it.

To demonstrate the idea we did two experiments. First was based on features extracted from co-occurrence matrices computed from all four bands. In the second test we used features derived from only the low-low frequency band (i.e., a subset of the features used in the first test). The results we obtained were in compliance with the assumptions we made. Using subband domain features (as we called) increased the detection rates compared to the features derived from spatial domain co-occurrence matrices. Using only the low-low band features improved the performance further. In the following we give in a formal language what we have discussed in hitherto.

3.7.1. The Algorithm

Given an image $I(n,m)$ of size 256x256 to extract subband domain features apply the following steps.

i- Decompose image $I(n,m)$ into four bands using wavelet filter coefficients to obtain images I_{LL}, I_{LH}, I_{HL} and I_{HH}.

ii- Calculate energy e_x of each decomposed image as:

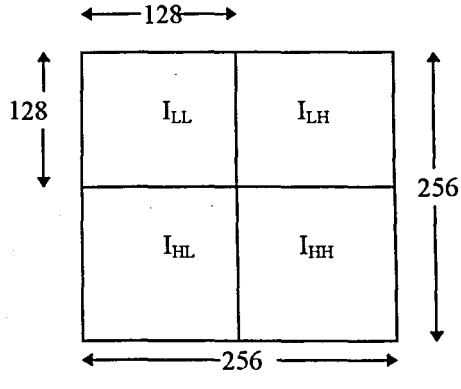

$$e_x = \frac{1}{N^2} \sum_n \sum_m |I_x(n,m)|$$

where N=128 and x denotes LL, LH, HL and HH bands.

iii-If energy of a decomposed image is significantly low than the energy with maximum value discard this band and consider only the remaining. That is, consider bands with $e_x > Ce_{max}$. C is a constant less than one.

iv- Divide each subband image into nonoverlapping subwindows $S_{x,i}$ of size 16x16. Indices x and i denote subband and subwindows respectively ($1 \leq i \leq 64$).

v- Derive the co-occurrence matrices P_θ for d =1 (pixel separation distance) and angles $\theta = (0, \pi/4, \pi/2, 3\pi/4)$ radians .

vi-Calculate ENT, CON, ASM, IDM for each co-occurrence matrix as in equations (2.2)-(2.5).

vii-Compute mean μ_X and standard deviation σ_X for each feature of four angles.

viii- Construct the vector

$$\mathbf{f}_{x,i} = [\mu_{ENT}\ \sigma_{ENT}\ \mu_{CON}\ \sigma_{CON}\ \mu_{ASM}\ \sigma_{ASM}\ \mu_{IDM}\ \sigma_{IDM}].$$

ix-Repeat steps (v) to (viii) for all bands (x) being retained according to the argument in step (iii) .

x- Feature vector for i'th subwindow corresponding to a region of size 32x32 in the original image is constructed as :

$$\mathbf{x}_i = [\ \mathbf{f}_{LL,i}\ \mathbf{f}_{LH,i}\ \ldots.]^T.$$

xi- Repeat steps (v) to (x) for all i.

3.7.2. Implementation and Results

We applied the given algorithm to our database. For decomposing the raw image we used Battle-Lemarie wavelet filter coefficients. Before computing the co-occurrence matrices we quantized each subimage into 8-levels. Value of constant C was chosen to be 0.35. For this value all bands except the LL band were discarded. We repeated the tests decreasing C such that all four bands are considered. In Table 3.5 we give the detection rates for each defect type for these two extreme cases (i.e., single band and all bands). Results as we outlined show that using only lower resolution images is sufficient. Hence 0.35 is a good selection. When compared with the spatial domain co-occurrence features we observe one-three per cent increase in the overall detection rate. But it should be noticed that one-three per cent improvement in the detection rate corresponds to 10-30 per cent increase in the correct detection rate (see Figure 3.22) or by the same amount decrease in the false alarm rate since amount of defective subwindows is only one-tenth of the total regions tested. Figure 3.19 contains the plot of average and best achievable detection rates for each defect type. While in Figure 3.20 SOC curves for both spatial domain co-occurrence matrices (SDCM) and subband domain co-occurrence matrices (SBCM) are shown on the same graph. Finally Figure 3.21 illustrates SOC curves at the presence of each defect type separately.

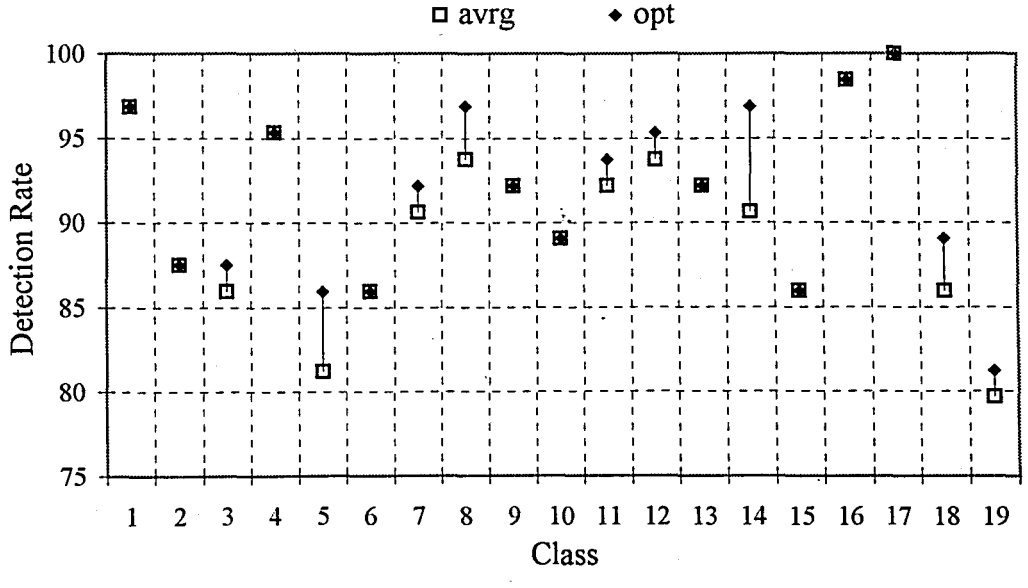

FIGURE 3.19. Average and best achievable detection rates using SBCM features.

TABLE 3.5. Performance of the SBCM based defect detection algorithm

	Detection Rates (%)	
Defect Class	ALL 4-BANDS	LL-BAND
dc1	96.88	96.88
dc2	89.06	87.50
dc3	84.38	85.94
dc4	96.88	95.31
dc5	81.25	81.25
dc6	81.25	85.94
dc7	85.94	90.63
dc8	93.75	93.75
dc9	92.19	92.19
dc10	87.50	89.06
dc11	90.63	92.19
dc12	89.06	93.75
dc13	92.19	92.19
dc14	92.19	90.63
dc15	84.38	85.94
dc16	98.44	98.44
dc17	100.00	100.00
dc18	90.63	85.94
dc19	82.81	79.69
Average	90.31	90.78

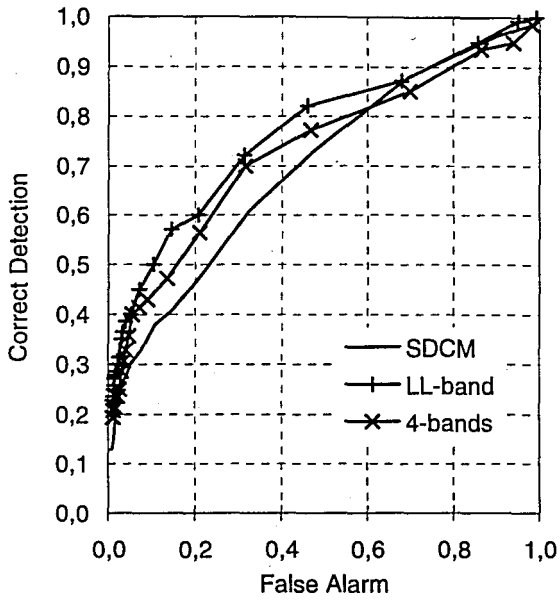

FIGURE 3.20. Average SOC curves for SDCM and SBCM based systems.

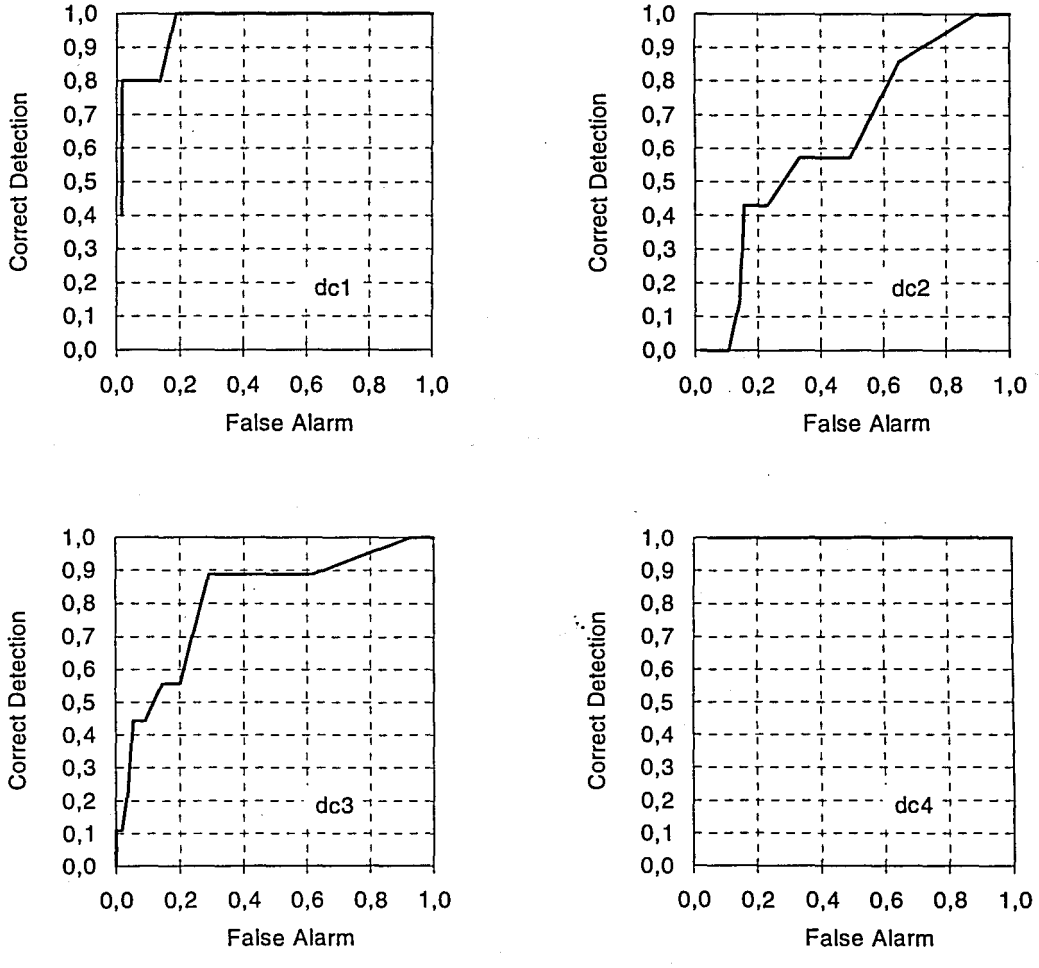

FIGURE 3.21. SOC curves for SBCM based system under each defect type.

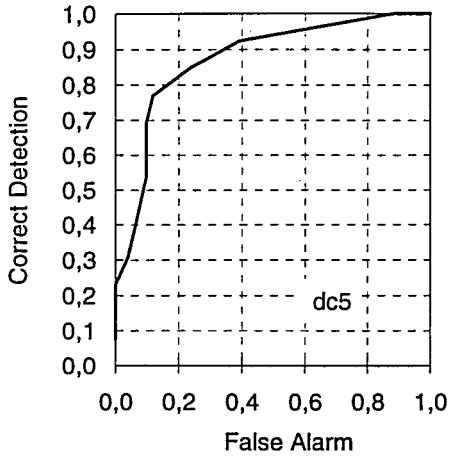

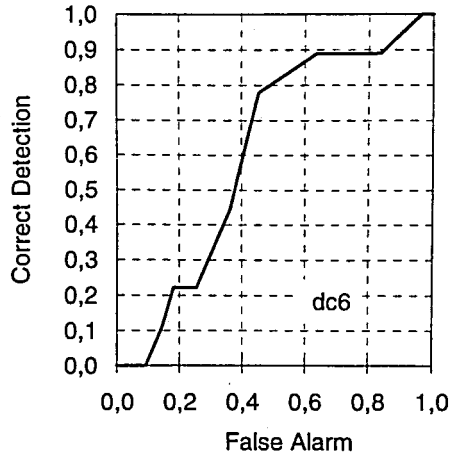

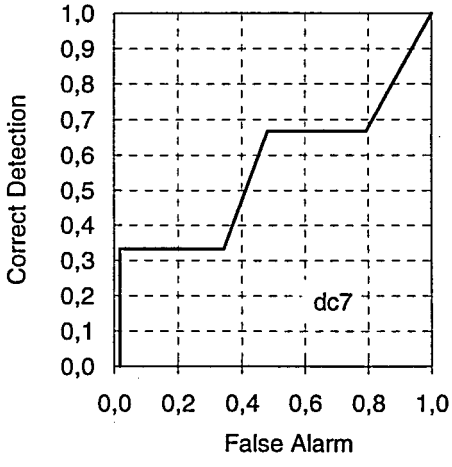

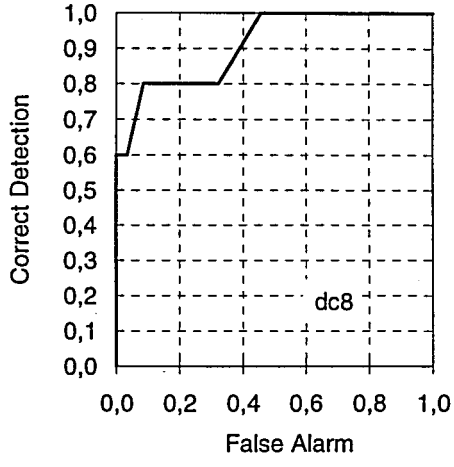

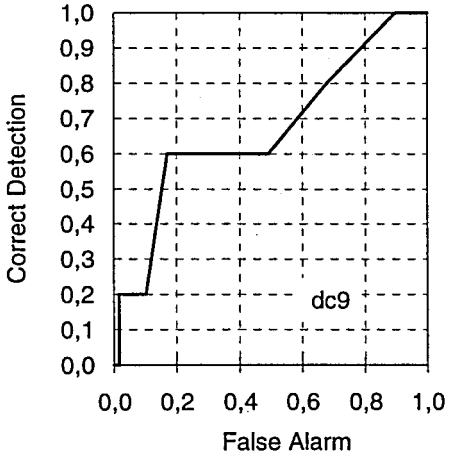

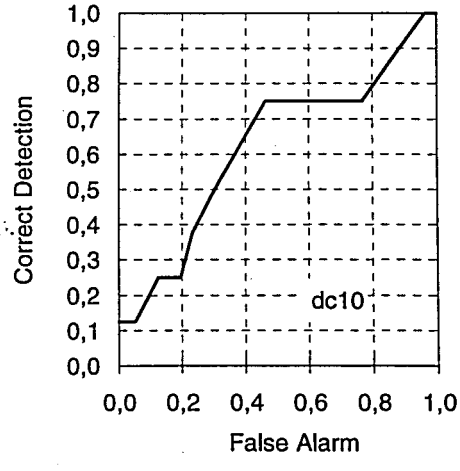

FIGURE 3.21. (continued)

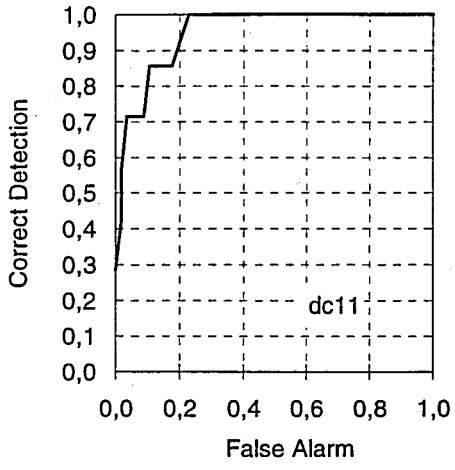

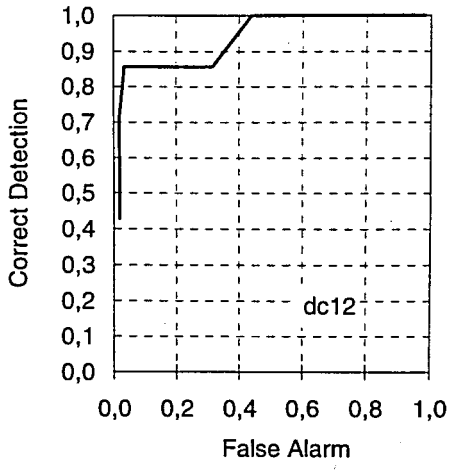

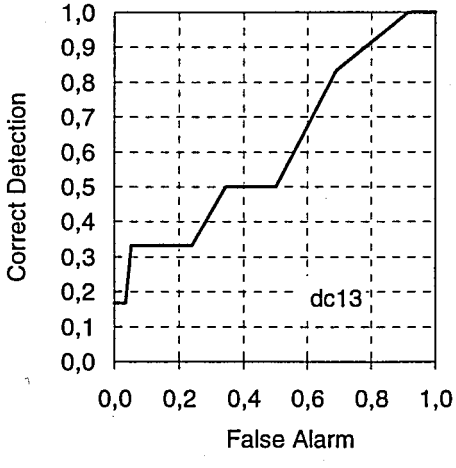

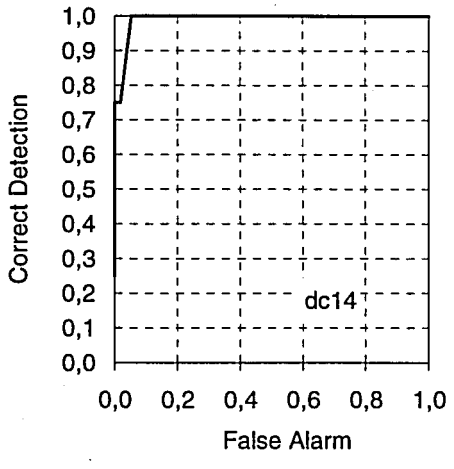

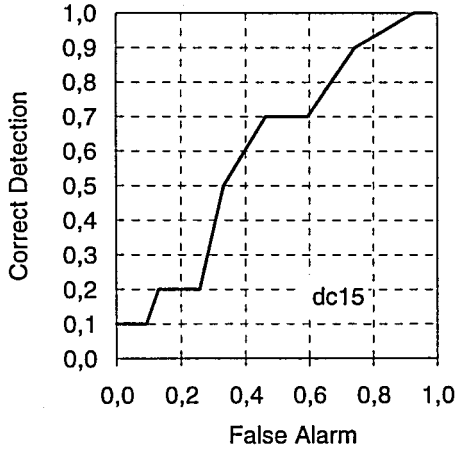

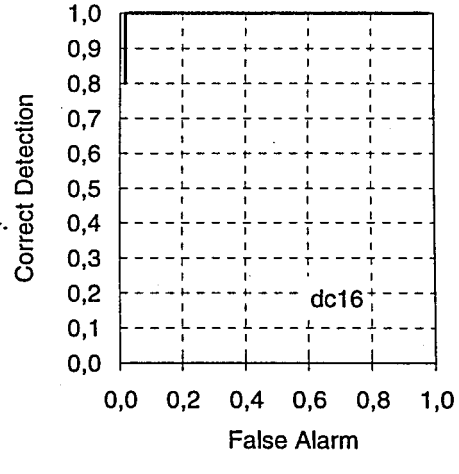

FIGURE 3.21. (continued)

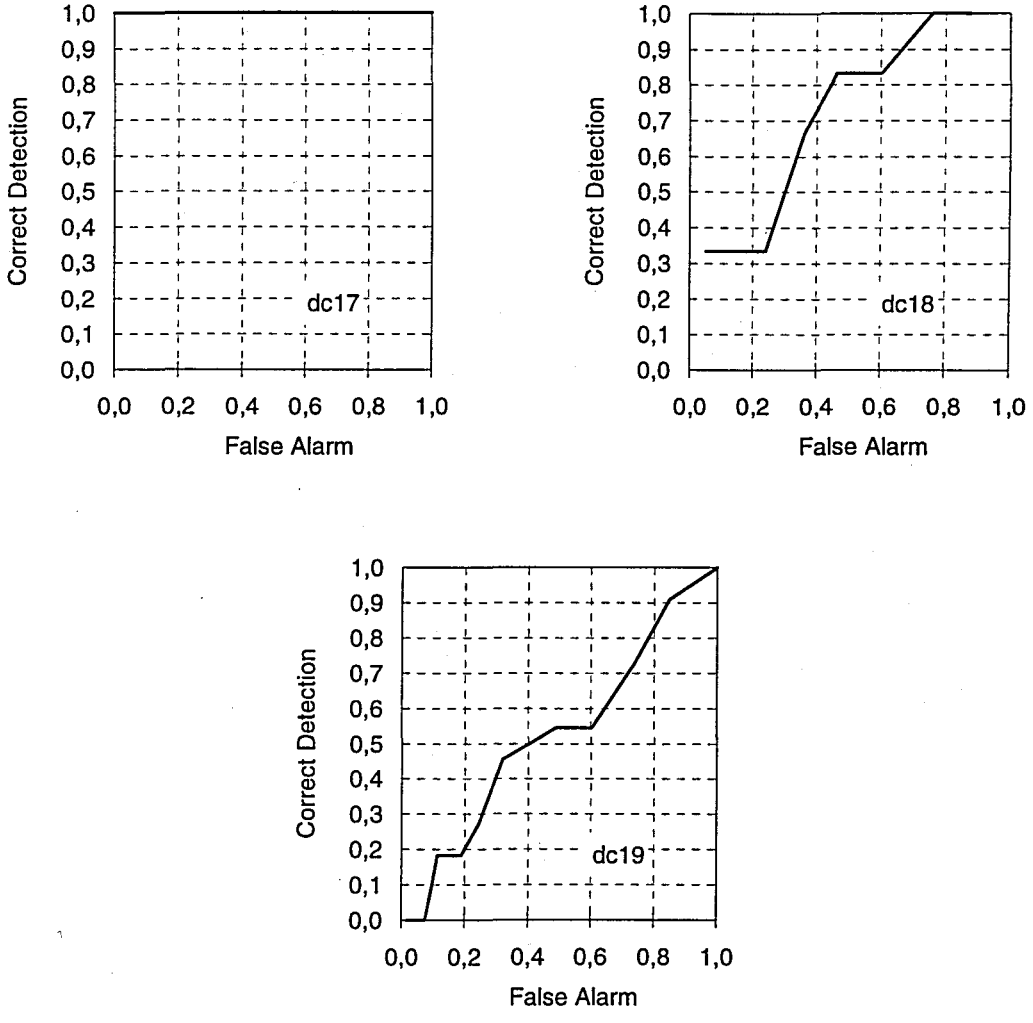

FIGURE 3.21. (continued)

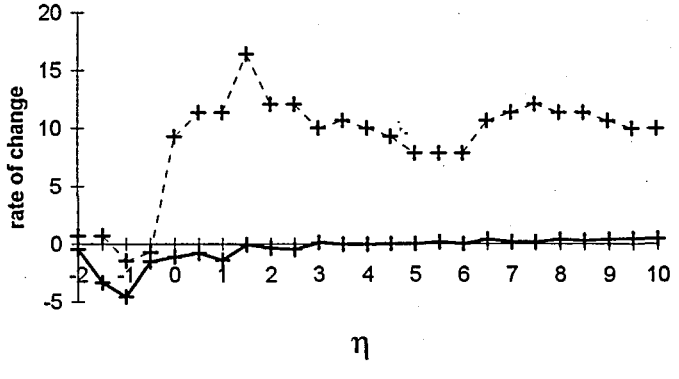

FIGURE 3.22. Increase in the correct detection rate (dashed line) and decrease in false alarm rate (solid line) for different values of constant (η) obtained with SBCM over SDCM.

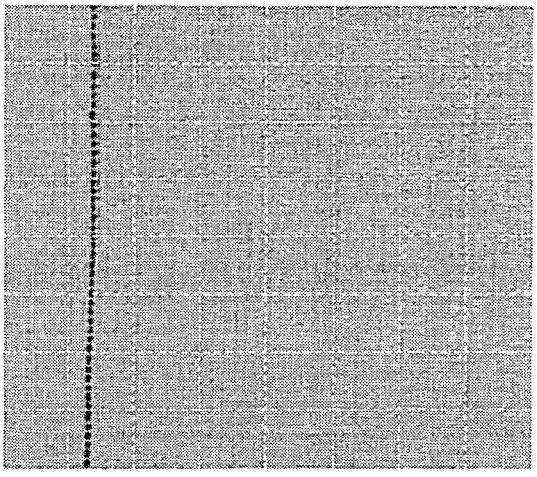

FIGURE 3.23. Defective textile fabric image 'dc17'

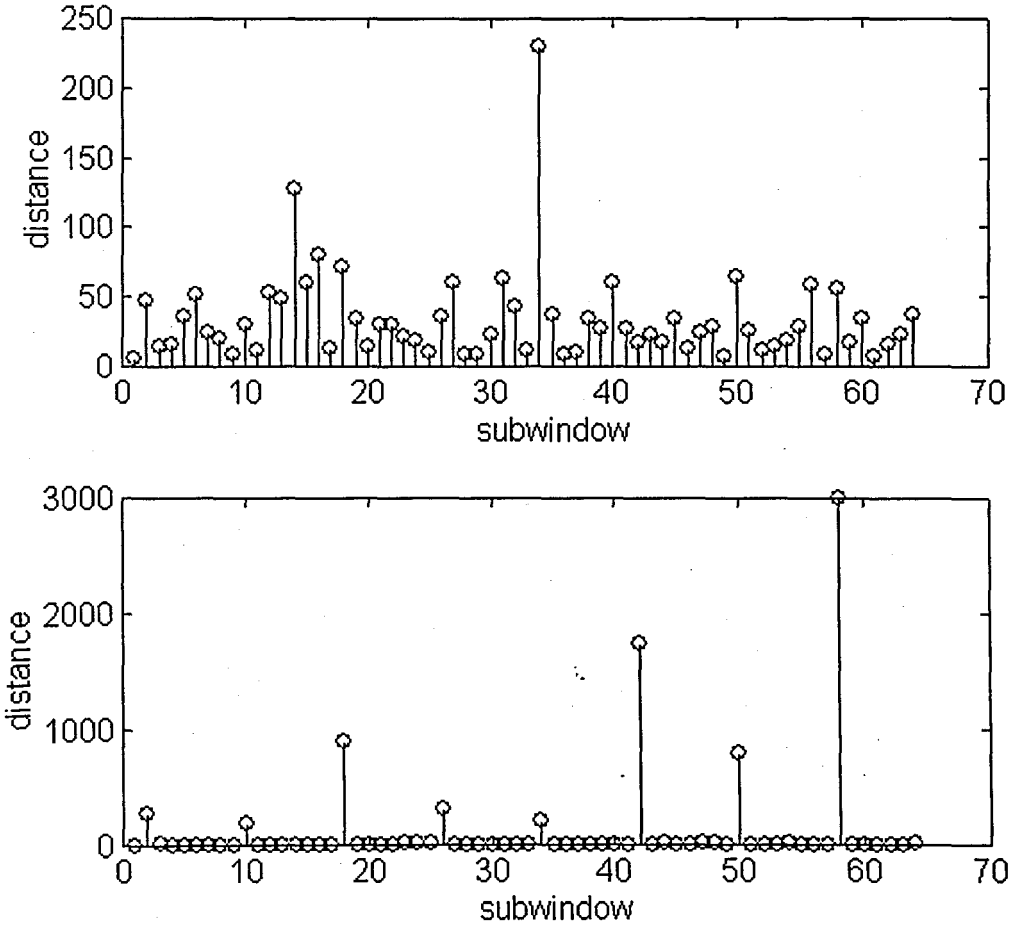

FIGURE 3.24. Distance (d_i)values for the subwindows (i) of defective textile fabric image 'dc17' obtained using SDCM (top) and SBCM methods (bottom).

3.7. Comparison of the Algorithms in terms of Computational Complexity and Performance

Examining the results, what they imply is that 2-level decomposition does not seem to be adequate to extract features with good discrimination power for a defect detection system based on partitioning of an image into subregions and searching for defects within those subimages. The reason is that as the image size gets comparable with the filter length, the averaging effect of the filter becomes so dominant as to smooth out the image. To overcome this problem, the subwindow size should be increased. But this results in missing of defects when they occupy only a small portion of the window. Resolution of this dichotomy seems to lie on selection of different strategy in locating defected parts (e.g., in pixel base).

Comparing pyramid structured wavelet transform with the wavelet packet signatures, we observe that in terms of performance they are almost the same. This, as we have shown, is due to the lowpass nature of the defected textures. Additional decomposition of the high frequency bands does not bring any advantage than increase in the computational requirements (see Table 3.6). This is verified also with the case of subband domain co-occurrence matrices. Where selecting a smaller feature set computed considering only the lower resolution image gives better detection rates than that obtained using all four bands.

Multichannel Gabor filters have been once more proven to be the optimum in term of spatial/spatial-frequency localization. Detection capacity of multifrequency energy features derived from Gabor filtered images is apparent in the SOC curves (Figure 3.15). In the experiments we carried out, most of the defects were detected with relatively small false alarm rates. However, when computational and storage requirements are concerned one can not talk about the same optimality. The computational demand is approximately as much as 100 times that of wavelet transform based method. A possible remedy is to reduce the filter set by incorporating feature selection or parameter tuning algorithm as suggested in [25]and [27]. But even if using a single filter, the computational requirement can not be less

than that of WPS based system. Moreover, the experiments we did by selecting different subsets from the 28 filters that we used have all resulted in a drop of considerable amounts in the detection rates.

Alternative for multifrequency features we proposed subband domain co-occurrence matrices (SBCM). Computationally, this method is superior to the first three that we discussed above (i.e., PSWT, WPS and Gabor). In terms of false alarm and correct detection rates it is ranked immediately after the Gabor filtering method (Figure 3.23). The sole disadvantage is the selection of feature set. The features we used may not yield good results for textures with very unlike characteristics. Nonetheless, our purpose here was to make an initial study to assess wavelet transform features for texture defect detection and not to design a complete system therefore we did not deal with fine tuning of the algorithm. In a sense we compared (in terms of defect detection) features derived using two approaches to texture modeling: statistical (SDCM) and signal processing (PSWT, WPS, Gabor) and a hybrid of both (SBCM). Finally to achieve completeness we included test results of the application of Markov Random Fields (MRF) to our database as a representative of the model based methods and to test the idea of subband domain features we applied MRF's to subband images. Since here is not the place to introduce a new algorithm what we can say is that we just applied the method discussed in [44] to extract features and used our own classifier to detect defective subregions each of size 32x32 represented by a feature vector of length 25 computed from the sufficient statistics of a ninth order MRF model. For subband MRF's (SBMRF) on the other hand we used 16x16 subwindows to extract ninth order MRF features from low-low band images obtained by decomposition of the original 256x256 sized fabrics into four bands using Battle-Lemarie filters. SOC curves and detection rates about all methods are plotted in the Figures 3.25 and 3.26 respectively. Computational requirements of each method are summarized in Table 3.6. Derivation of the formulas are provided in appendix-A.

TABLE 3.6. Computation requirements for feature extraction in an image of size 256 by 256.

METHOD	ADDITIONS ($\times 10^6$)	MULTIPLICATIONS ($\times 10^6$)
PSWT	2.52	2.62
WPS	4.00	4.20
Gabor	383.51	763.36
SDCM	0.46	0.18
SBCM	0.96	0.92
MRF	1.64	1.64
SBMRF	1.15	1.20

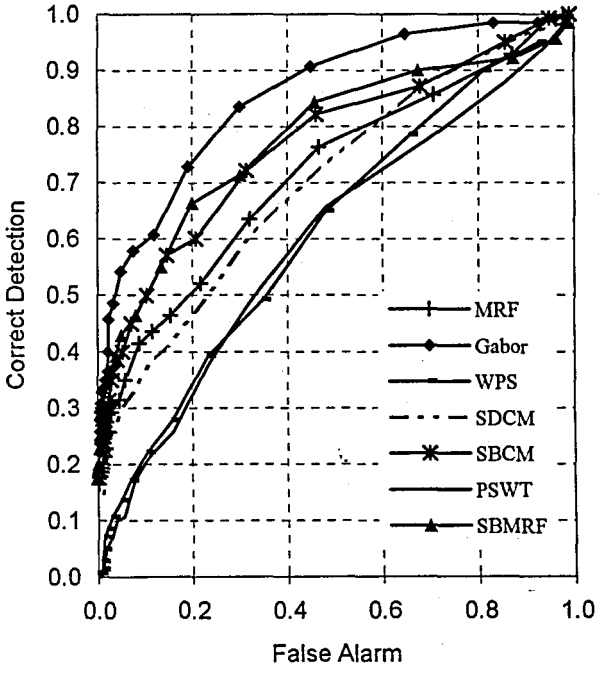

FIGURE 3.25. SOC curves for all methods

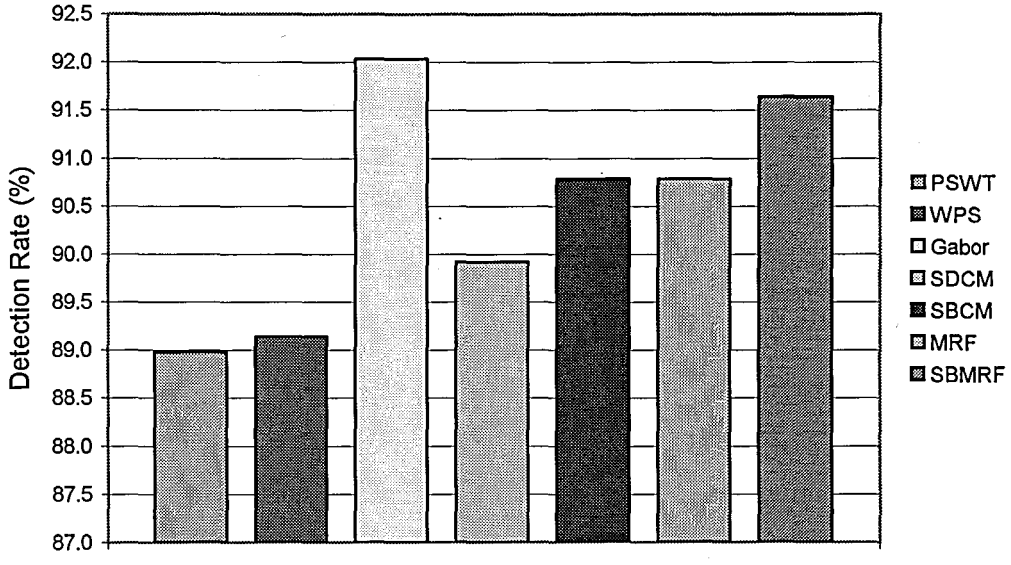

FIGURE 3.26. Performance of each method

4. CONCLUSION

In this thesis we investigated the defect detection problem in textured images. As we pointed out texture analysis is a difficult yet rich subject with many fields of application. One such a field is the visual inspection of industrial products. So we concentrated on the defect detection of textile fabric images.

We applied five different methods for the solution of this difficult problem. The results we obtained differ from 85 to 92 per cent. Slight variants of these methods can be found in the literature [19],[20],[36],[51] applied for the texture classification problem , with performances ranging from 95 to 100 per cent. In the classification and identification problems features are derived from local windows with single class so the feature space tends to form clusters, whereas in the defect detection, due to the nature of the problem, most of the time the features derived from the defective subwindows are not clustered but split around or even within the feature space of nondefective windows, depending on the type and size of the defect.

From all the five methods we implemented, the best results were obtained with the features derived from the gabor filtered images. Gabor filters as we mentioned, have been shown [39] to be optimal in terms of spatial/spatial-frequency localization, and experimentally, found to be the best approximate of the cortical receptive field models of mammals [40],[52]. But their huge computational and storage requirements makes their use in real time systems almost impossible. Most interesting and attractive method was the one based on the subband domain features. This at first side appears to be strange when compared with the performance of spatial domain features. One expects decrease in performance, since features are derived from lower resolution images. But if we consider textures with frequency content mostly concentrated on a single band focusing on that particular band and discarding the others which carry information with low discriminatory power improves the detection performance, which can be considered as a case of what is called selective attention in psychology. This makes them appealing not only due to the remarkable computational improvement they provide over the gabor filtering based

method but also due to their performance which is very close to that of the gabor filtering based method found to be the best.

In this respect, as future work, we think a more elaborate study of model based methods as Markov Random Fields or Higher Order Statistics, in the subband domain would be reasonable since it will enable reduction in the model order which means improvement in the computational complexity and at the same time improvement of the performance. Our first experiments, which we did include here, with the Markov random field models were supporting this claim.

Concluding we could say, among all methods we have studied, the one that we proposed, based on subband domain features seems to be the most suitable for the automated inspection of the textile fabrics against majority of the defects. Finally, we hope, by the improvement of the texture analysis methods, in the near future, algorithms of academic interest today will be part of real time inspection systems in industry and consumer products in the market.

APPENDIX A : COMPUTATIONAL COMPLEXITY CALCULATIONS

For an image $I(n,m)$ of size NxN the computational requirements for the following signal processing operations are as follows :

A- Quantization : Scalar quantization of an image $I(n,m)$ into G levels simply can be approximated by the following operations :

$$\Delta = (I_{max}-I_{min})/G\ ,\ I_Q(n,m)=\lfloor\{I(n,m)-I_{min}\}/\Delta\rfloor;$$

where I_{max} and I_{min} are maximum and minimum gray values in $I(n,m)$) and are assumed to be known and $\lfloor X \rfloor$ denotes maximum integer less than or equal to X;

Total # of additions = N^2+1; Total # of multiplications = N^2+1;

B- One-Level Decomposition : In one-level decomposition of an image (i.e. splitting into four bands) with separable filters of length L for a single band total number of additions and multiplications are as following :

Total # of additions = $(3/4)\,N^2\,(L-1)$; Total # of multiplications = $(3/4)\,N^2\,L$;

C- 2D- Discrete Filtering : Filtering of an image $I(n,m)$ of size NxN with a filter $h(n,m)$ of size LxL requires $N^2\,L^2$ multiplications and $N^2\,(L^2-1)$ additions when this is performed with 2-D circular convolution. However, the computational complexity, when FFT routines are used becomes: $Q^2[3\log_2\{Q^2\}+1]$ complex multiplications or $4Q^2[3\log_2\{Q^2\}+1]$ real multiplications and $2Q^2[3\log_2\{Q^2\}+1]$ additions with Q satisfying $Q > N^2 + L^2 - 1$ and $Q = 2^\gamma$ where γ is integer.

(Recall that 2D-FFT of an MxN sized data matrix requires $MN\log_2 MN$ complex multiplications [53],[54],[55]).

D- Co-occurrence Matrices : Computation of GxG gray level co-occurrence matrices for a displacement vector $\mathbf{d}=(dx,dy)$ requires $(N-dx)(N-dy)$ additions.

E- Texture Features : Computational requirements for textural features derived from image gray levels directly or calculated from the co-occurrence matrices are summarized in Table A.1.

TABLE A.1. Computational Complexity of Textural Features

FEATURE	EXPRESSION	ADDITIONS	MULTIPLICATIONS
Energy	$\frac{1}{N^2}\sum_n\sum_m\{I(n,m)\}^2$	N^2-1	N^2+1
Energy (l1-norm)	$\frac{1}{N^2}\sum_n\sum_m\lvert I(n,m)\rvert$	N^2-1	1
Entropy	$-\sum_i\sum_j p(i,j)\log p(i,j)$	G^2-1	G^2 +1
Contrast	$\sum_i\sum_j (i-j)^2 p(i,j)$	2 G^2-1	2 G^2
Angular Second Moment	$\sum_i\sum_j\{p(i,j)\}^2$	G^2-1	G^2
Inverse Difference Moment	$\sum_i\sum_j\frac{1}{1+(i-j)^2}p(i,j)$	$3G^2$-1	$3G^2$

APPENDIX B: DEFECTED TEXTURE SET

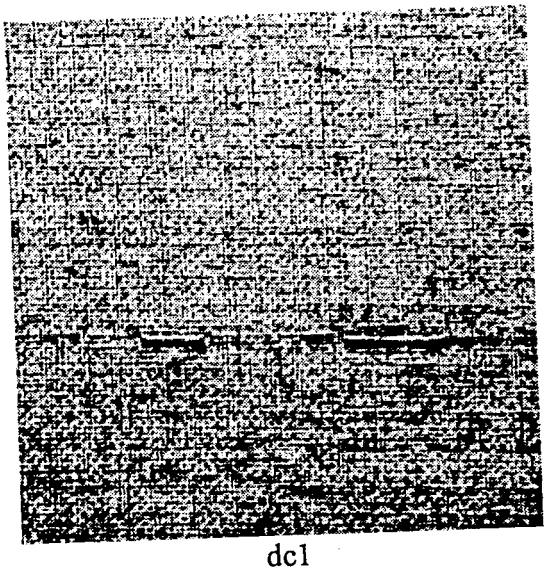

dc1

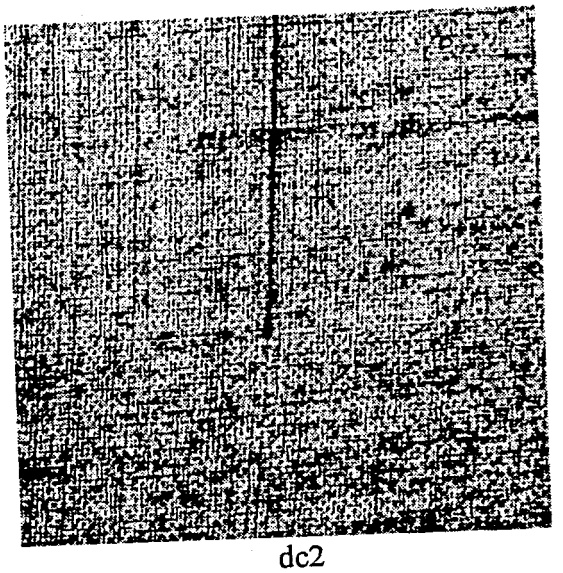

dc2

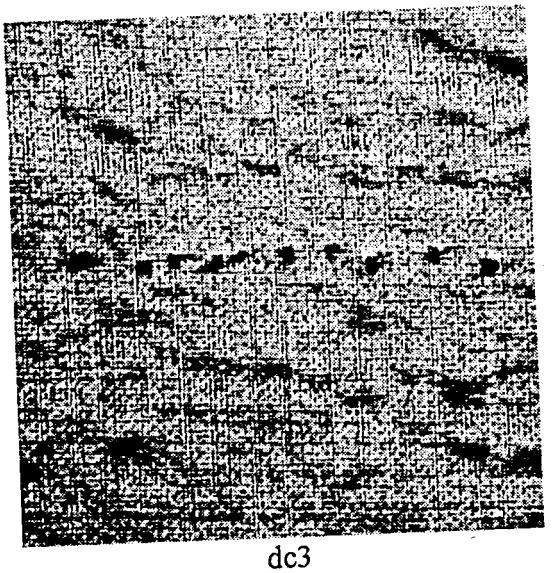

dc3

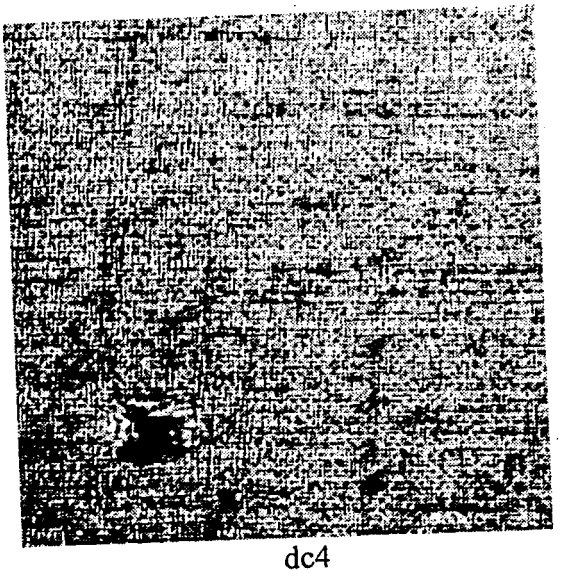

dc4

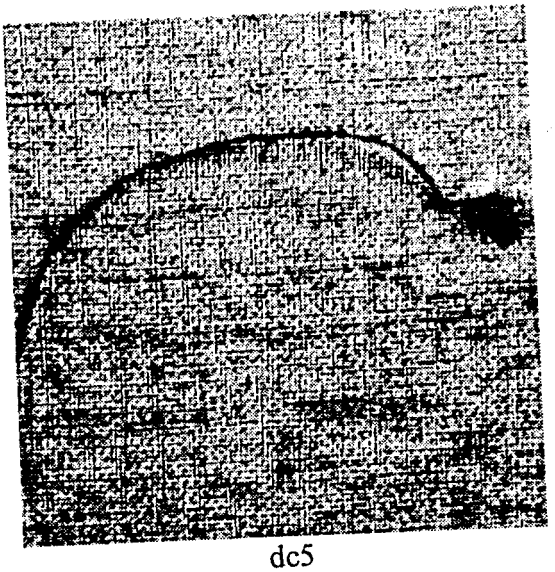

dc5

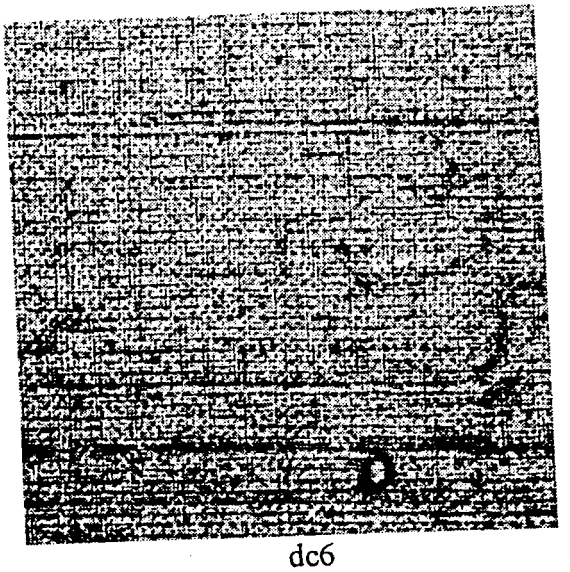

dc6

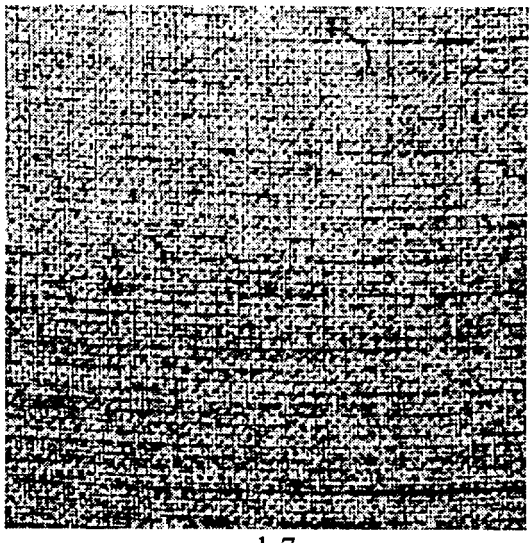

dc7

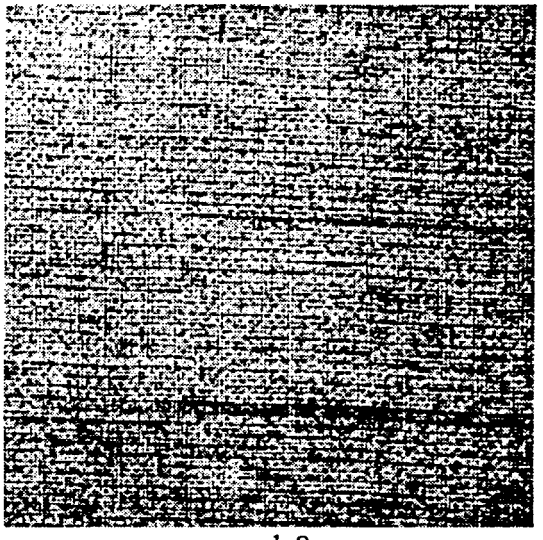

dc8

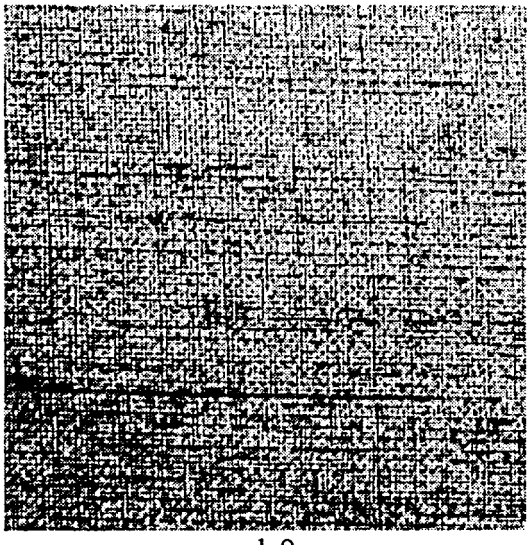

dc9

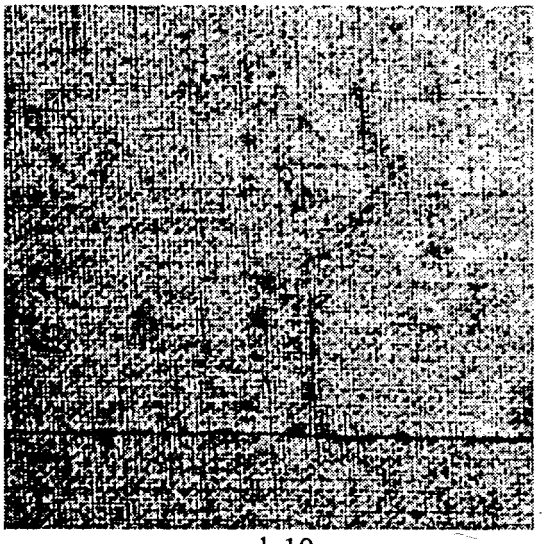

dc10

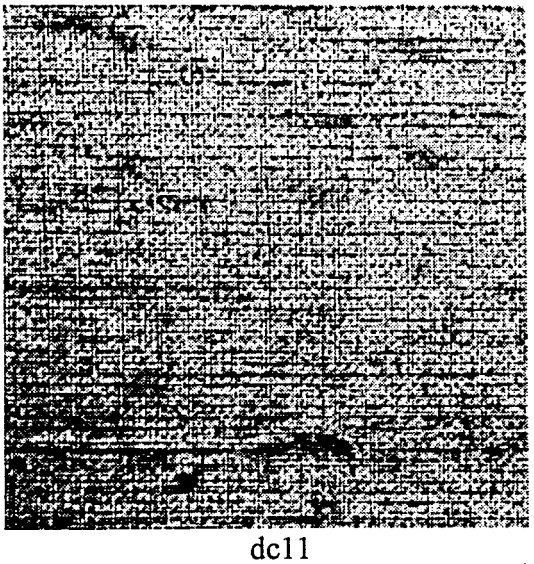

dc11

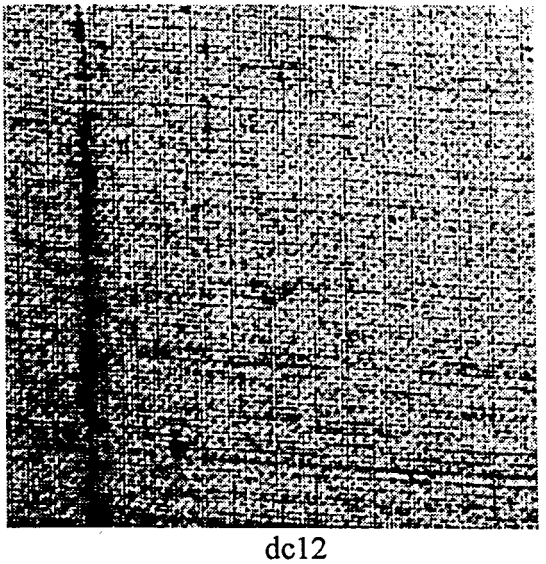

dc12

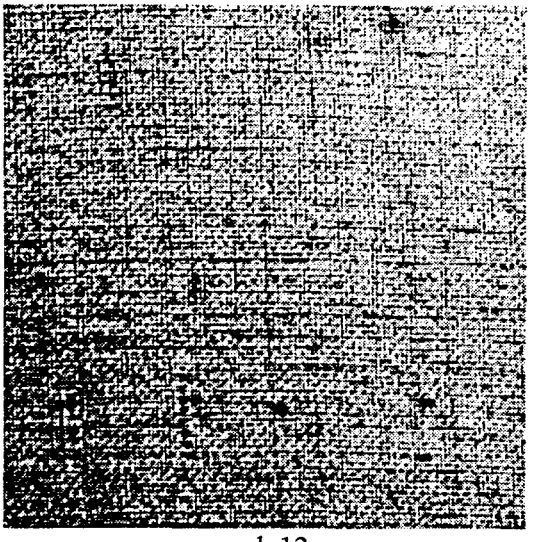

dc13

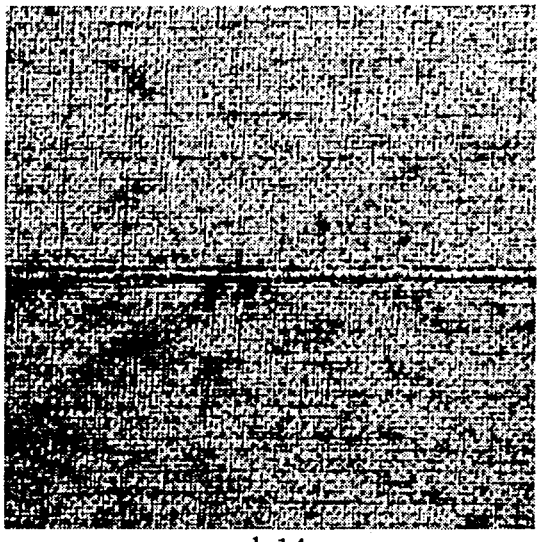

dc14

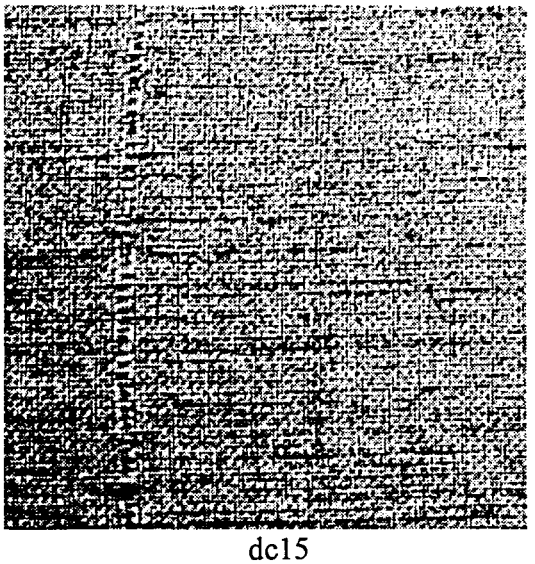

dc15

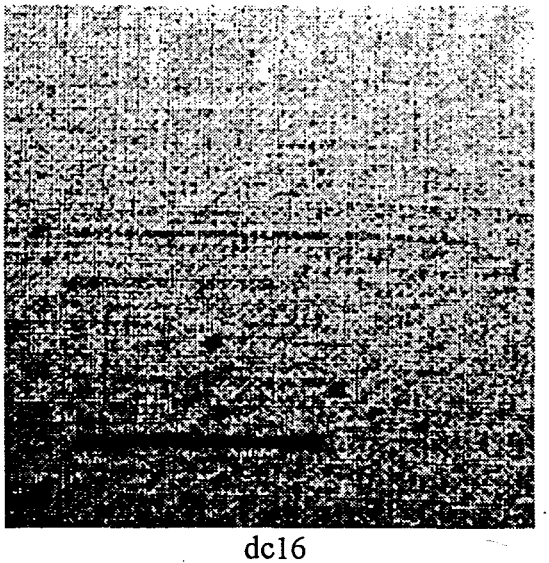

dc16

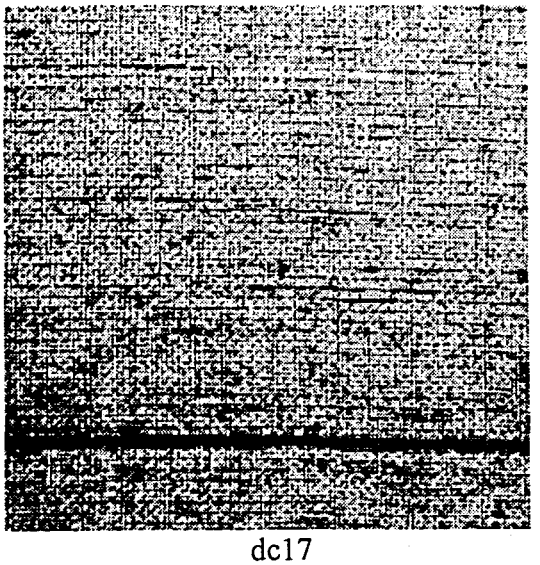

dc17

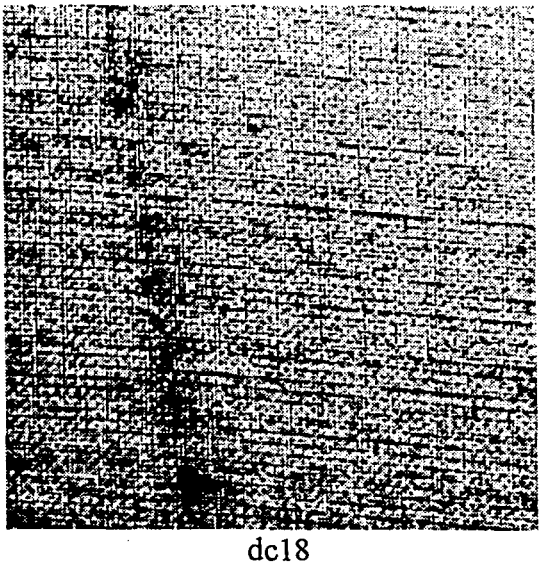

dc18

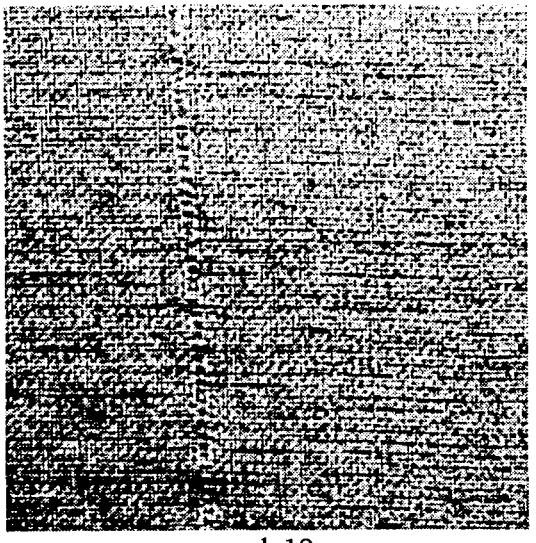

dc19

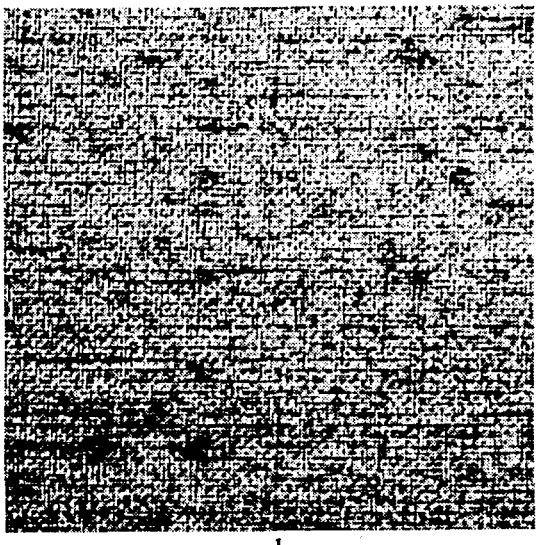

clean

REFERENCES

1. Smith, B., "Making War on Defects : Six-Sigma Design," *IEEE Spectrum,* Vol. 30, No. 9, pp. 43-47, September 1993.

2. Neukermans, A., "The Current State of the Art of Defect Detection Using Laser Scanning Systems," *Proceedings of the Symposium on Control, Defect Reduction Semiconductor Manufacturing,* Toronto-Canada , pp. 112-133, 1992.

3. Zmola, C., A. Segal, B. Lovewell and C. Nash, "Adaptive Texture Filtering for Defect Inspection in Ultrasound Images," *Proc. SPIE 1907*, pp. 133-138, 1993.

4. Brzakovic, D. and N. Vujovic, "Designing a Defect Classification System: A Case Study," *Pattern Recognition,* Vol. 29, No. 8, pp. 1401-1419, August 1996.

5. Hawkins, J. K., "Textural Properties for Pattern Recognition," in B. Lipkin and A. Rosenfeld (Eds.), *Picture Processing and Psychopictorics*, Academic Press, New York, 1969.

6. Horn, B. K. P., *Robot Vision*, McGraw-Hill, New York, 1986.

7. Sklansky, J., "Image Segmentation and Feature Extraction," *IEEE Transactions on Systems, Man, and Cybernetics*, Vol. 8, pp. 237-247, 1978.

8. Tuceryan, M. and A. K. Jain, "Texture Analysis," in C. H. Chen, L. F. Pau and P.S.P. Wang (Eds.), *The Handbook of Pattern Recognition and Computer Vision*, World Scientific, River Edge, NJ, 1993.

9. Van Gool, L., P. Dewaele and A. Oosterlinck, "Texture Analysis Anno 1983," *Comput. Vision, Graphics, Image Processing*, Vol. 29, pp. 336-357, 1985.

10. Haralick, R. M., "Statistical and Structural Approaches to Texture," *Proceedings of IEEE*, Vol. 67, No. 5, pp. 786-804, May 1979.

11. Zucker, S.W., A. Rosenfeld and L.S. Davis, "Picture Segmentation by Texture Discrimination," *IEEE Transactions on Computers*, Vol. C-24, pp. 1218-1233, December 1975.

12. Tomita, F., Y. Shirai and S. Tsuji, "Description of Textures by a Structural Analysis," *IEEE Transactions on Pattern Analysis and Machine Intelligence*, Vol. 4, pp. 183-191, 1982.

13. Cross, G.R. and A.K. Jain, "Markov Random Field Texture Models," *IEEE Transactions on Pattern Analysis and Machine Intelligence*, Vol. 5, pp. 25-39, 1983.

14. Derin, H. and W.S. Cole, "Segmentation of Textured Images Using Gibbs Random Fields," *Comput. Vision, Graphics, Image Processing*, Vol. 35, pp. 72-98, 1986.

15. Kashyap, R.L. and A. Khotanzad, "A Model-Based Method for Rotation Invariant Texture Classification," *IEEE Transactions on Pattern Analysis and Machine Intelligence*, Vol. 8, No. 4 pp. 472-481, 1986.

16. Mao, J. and A.K. Jain, "Texture Classification and Segmentation Using Multiresolution Simultaneous Autoregressive Models," *Pattern Recognition*, Vol. 25, No. 2, pp. 173-188, 1992.

17. Bouman, C. and B. Liu, "Multiple Resolution Segmentation of Textured Images," *IEEE Transactions on Pattern Analysis and Machine Intelligence*, Vol. 13, No. 2, pp. 99-113, 1991.

18. Keller, J. M and R. M. Crownover, "Texture Description and Segmentation Through Fractal Geometry," *Comput. Vision, Graphics, Image Processing*, Vol. 45, pp. 150-166, 1989.

19. Laine, A. and J. Fan, "Texture Classification by Wavelet Packet Signatures," *IEEE Transactions on Pattern Analysis and Machine Intelligence*, Vol. 15, No. 11, pp. 1186-1191, November 1993.

20. Chang, T. and C.-C. Jay Kuo, "Texture Analysis and Classification with Tree-Structured Wavelet Transform," *IEEE Transactions on Image Processing*, Vol. 2, No. 4, pp. 429-441, October 1993.

21. Daugman, J. G., "Complete Discrete 2-D Gabor Transforms by Neural Networks for Image Analysis and Compression," *IEEE Transactions on Acoustics, Speech, and Signal Processing*, Vol. 36, No. 7, pp. 1169-1179, July 1988.

22. Turner, M.R., "Texture Discrimination by Gabor Functions," *Biological Cybernetics*, Vol. 55, pp. 71-82, 1986.

23. Bovik, A.C., M. Clark and W.S. Geisler, "Multichannel Texture Analysis Using Localized Spatial Filters," *IEEE Transactions on Pattern Analysis and Machine Intelligence*, Vol. 12, No. 1, pp. 55-73, January 1990.

24. Bovik, A.C. , "Analysis of Multichannel Narrow-Band Filters for Image Texture Segmentation," *IEEE Transactions on Signal Processing*, Vol. 39, pp. 2025-2043, September 1991.

25. Jain, A.K. and F. Farrokhnia, "Unsupervised Texture Segmentation Using Gabor Filters," *Pattern Recognition*, Vol. 24, No. 12, pp. 1167-1186, December 1991.

26. Dunn, D., W. E. Higgins and J. Wakely, "Texture Segmentation Using 2-D Gabor Elementary Functions," *IEEE Transactions on Pattern Analysis and Machine Intelligence*, Vol. 16, No. 2, pp. 130-149, February 1994.

27. Teuner, A., O. Pichler and B. J. Hosticka, "Unsupervised Texture Segmentation of Images Using Tuned Matched Gabor Filters," *IEEE Transactions on Image Processing*, Vol. 4, No. 6, pp. 863-870, June 1995.

28. Julesz, B., "Visual Pattern Discrimination," *IRE Transactions on Information Theory*, pp. 84-92, February 1962.

29. Haralick, R. M., K. Shanmugan and I. Dinstein, "Textural Features for Image Classification," *IEEE Transactions on Systems, Man and Cybernetics*, Vol. SMC-3, No. 6, pp. 610-621, November 1973.

30. Siew, L.H., R.M. Hodgson and E.J. Wood, "Texture Measures for Carpet Wear Assessment," *IEEE Transactions on Pattern Analysis and Machine Intelligence*, Vol. 10, No. 1, pp. 92-105, January 1988.

31. Weszka, J.S., C.R. Dyer and A. Rosenfeld, "A Comparative Study of Texture Measures for Terrain Classification," *IEEE Transactions on Systems, Man and Cybernetics*, Vol. SMC-6, pp. 269-285, April 1976.

32. Ohanian, P.P and R.C. Dubes, "Performance Evaluation for Four Classes of Textural Features," *Pattern Recognition*, Vol. 25, No. 8, pp. 819-833, August 1992.

33. Daubechies, I., "Orthonormal Bases of Compactly Supported Wavelets," *Communications on Pure and Applied Mathematics*, Vol. 41, pp. 909-996, November 1988.

34. Mallat, S. G., "A Theory for Multiresolution Signal Decomposition: The Wavelet Representation," *IEEE Transactions on Pattern Analysis and Machine Intelligence*, Vol. 11, No. 7, pp. 674-693, July 1989.

35. Coifman, R.R. and M.V. Wickerhauser, "Entropy Based Algorithms for Best Basis Selection," *IEEE Transactions on Information Theory*, Vol. 38, No. 3, pp. 713-718, March 1992.

36. Etemad, K. and R. Chellappa, "Separability Based Tree Structured Local Basis Selection for Texture Classification," *IEEE International Conference on Image Processing* (ICIP'94), Vol. III, pp. 441-445, Austin-Texas, 1994.

37. Lee, C.S, C.-H. Choi, J.Y. Choi, Y.K. Kim and S.H. Choi, "Feature Extraction Algorithm Based on Adaptive Wavelet Packet for Surface Defect Classification," *IEEE International Conference on Image Processing* (ICIP'96), Vol. II, pp. 673-675, 1996.

38. Gabor, D., "Theory of Communication," *Journal of IEE*, Vol. 93, pp. 429-457, 1946.

39. Daugman, J.G., "Uncertainty Relation for Resolution in Space, Spatial Frequency, and Orientation Optimized by Two-Dimensional Visual Cortical Filters," *Journal of Optical Society of America*, Vol. 2, pp. 1160-1169, 1985.

40. Webster, M. A. and R.L. De Valois, "Relationship Between Spatial-Frequency and Orientation Tuning of Striate-Cortex Cells," *Journal of Optical Society of America*, Vol. 2, pp. 1124-1132, 1985.

41. Kulikowski, J.J., S. Marcelja and P. Bishop, "Theory of Spatial Position and Spatial Frequency Relations in the Receptive Fields of Simple Cells in the Visual Cortex," *Biological Cybernetics*, Vol. 43, pp. 187-198, 1982.

42. Chetverikov, D., "Texture Imperfections," *Pattern Recognition Letters*, Vol. 6, pp. 45-50, 1987.

43. Dewaele, P., P. Van Gool and A. Oosterlinck, "Texture Inspection with Self-Adaptive Convolution Filters," in *Proceedings of the 9th International Conference on Pattern Recognition*, Rome- Italy, Nov. 14-17, 1988, pp. 56-60.

44. Cohen, F.S., Z. Fan, and S. Attali, "Automated Inspection of Textile Fabrics Using Textural Models," *IEEE Transactions on Pattern Analysis and Machine Intelligence*, Vol. 13, No. 8, pp. 803-808, August 1991.

45. Neubauer, C., "Segmentation of Defects in Textile Fabric," in *Proceedings of the 11th International Conference on Pattern Recognition*, The Hague, The Netherlands, August 1992, pp. A.688-A.691.

46. Chen, J. and A.K. Jain, "A Structural Approach to Identify Defects in Textured Images," in *Proceedings of IEEE International Conference on Systems, Man, and Cybernetics*, pp. 29-32, Beijing, 1988.

47. Song, K.Y., M. Petrou and J. Kittler, "Texture Defect Detection: A Review," *SPIE Applications of Artificial Intelligence X: Machine Vision and Robotics*, Vol. 1708, pp. 99-106, 1992.

48. Newman, T.S. and A.K. Jain, "A Survey of Automated Visual Inspection," *Computer Vision and Image Understanding*, Vol. 61, No. 2, pp. 231-262, March 1995.

49. Daugman, J. G., "Two-Dimensional Spectral Analysis of Cortical Receptive Field Profile," *Vision Research*, Vol. 20, pp. 847-856, 1980.

50. Mallat, S., "Multifrequency Channel Decomposition of Images and Wavelet Models," *IEEE Transactions on Acoustics, Speech, and Signal Processing*, Vol. 37, No. 12, pp. 2091-2110, December 1989.

51 Pichler, O., A. Teuner and B. J. Hosticka, "A Comparison of Texture Feature Extraction Using Adaptive Gabor Filtering, Pyramidal and Tree-Structured Wavelet Transforms," *Pattern Recognition*, Vol. 29, No. 5, pp. 733-742, May 1996.

52. Tan, T. N., "Texture Edge Detection by Modelling Visual Cortical Channels," Pattern Recognition, Vol. 28, No. 9, pp. 1283-1298,1995.

53. Oppenheim, A.V. and R. W. Schafer, *Digital Signal Processing*, Englewood Cliffs, NJ: Prentice-Hall, 1975.

54. Brigham, E. O., *The Fast Fourier Transform and Its Applications*, Englewood Cliffs, NJ: Prentice-Hall, 1988.

55. Stearns, S. D. and R. A. David, *Signal Processing Algorithms*, Englewood Cliffs, NJ: Prentice-Hall, 1988.

REFERENCES NOT CITED

Akansu, A. N. and R. A. Haddad, *Multiresolution Signal Decomposition*, Academic Press Inc., Boston, 1992.

Brzakovic, D., H. Beck and N. Sufi, "An Appoach to Defect Detection in Materials Characterized by Complex Textures," *Pattern Recognition*, Vol. 23, No.1/2, pp. 99-107, 1990.

Duda, R. O., and P. E. Hart , *Pattern Classification and Scene Analysis*, John Wiley, New York, 1973.

Fukunaga, K., *Introduction to Statistical Pattern Recognition* (Second Edition), Academic Press Inc., San Diego, 1990.

Jain, A. K., *Fundamentals of Digital Image Processing*, Englewood Cliffs, NJ: Prentice-Hall, 1989.

Orr, R.S., "The Order of Computation for Finite Discrete Gabor Transforms," *IEEE Transactions on Signal Processing*, Vol. 41, No. 1, pp. 122-130, January 1993.

Porat, M. and Y. Zeevi, "The Generelized Gabor Scheme of Image Representation in Biological and Machine Vision," *IEEE Transactions on Pattern Analysis and Machine Intelligence*, Vol. 10, No. 4, pp. 452-468, 1988.

Rao, A. R., *A Taxonomy for Texture Description and Identification*, Springer-Verlag, New York, 1990.

Rioul, O. and P. Duhamel, "Fast Algorithms for Discrete and Continuous Wavelet Transforms," *IEEE Transactions on Information Theory*, Vol. 38, No. 2, pp. 569-586, March 1992.